REVIEW

Check for updates

Side-chain engineering of nonfullerene small-molecule acceptors for organic solar cells

Zhenghui Luo,* Tongle Xu, Cai'e Zhang [ID] and Chuluo Yang [ID] *

Thanks to their broad absorption spectra, easily modifiable molecular energy levels and chemical structures, nonfullerene small-molecule acceptors (SMAs) have attracted significant attention in the recent decade. To date, SMAs and polymer donor-based organic solar cells (OSCs) have achieved power conversion efficiencies (PCEs) of over 19%. During this time period, side-chain engineering has emerged as an effective method for enhancing the photovoltaic efficiency of the corresponding OSCs due to its simplicity and effectiveness in optimizing the physicochemical properties of nonfullerene SMAs. In this article, side-chain engineering of nonfullerene SMAs, including A–(π)–D–(π)–A-type SMAs and A–DA$_1$D–A-type SMAs, is summarized. The general methods for modifying the side chains of SMAs and their pivotal structure–performance relationships are combined and highlighted. The future challenges and prospects for the further side-chain optimization of the SMAs are proposed.

Broader context

Since 2015, the research field of organic solar cells (OSCs) has witnessed a significant growth of nonfullerene small-molecule acceptors (SMAs), and the power conversion efficiencies (PCE) of SMA-based binary OSCs have rapidly increased from 6% to 19%. Typically, nonfullerene SMAs consist of a central core, two or more terminal accepting units, and side chains. By manipulating central cores or terminal acceptor units, the optoelectronic properties of the molecules can be finely tuned, but the drawback is that manipulating these two parts is relatively time-consuming and complex as compared with modifying side chains. The "side-chain engineering" strategy is a direct, convenient and feasible method to optimize the chemical structures of molecules, and then effectively regulate the absorption, energy levels, solubility, electron mobility, and molecular interaction/aggregation, and therefore widely utilized in molecular design for OSCs. In this article, side-chain engineering of nonfullerene SMAs is summarized. The general methods for modifying the side chains of SMAs and their pivotal structure–performance relationships are combined and highlighted. The future challenges and prospects for the further side-chain optimization of the SMAs are proposed.

Shenzhen Key Laboratory of New Information Display and Storage Materials, College of Materials Science and Engineering, Shenzhen University, Shenzhen 518060, China. E-mail: zhhuiluo@szu.edu.cn, clyang@whu.edu.cn

Zhenghui Luo

Zhenghui Luo received his PhD degree in 2019 from Wuhan University, Wuhan, for his study in the field of organic photovoltaics under the guidance of Professor Chuluo Yang. From 2019 to 2021, he was a postdoctoral fellow in Professor He Yan's group at HKUST. Since 2022, he has been a full associate professor at Shenzhen University. His research interests focus on the synthesis and application of organic photovoltaic materials.

Chuluo Yang

Chuluo Yang received his PhD degree in organic chemistry from Wuhan University in 1997. From 1999 to 2002, he was a postdoctoral fellow at the Hong Kong University of Science and Technology, the University of New Orleans, and the University of Rochester. From 2003 to 2018, he was a full professor at Wuhan University. Since 2019, he has been a full professor at Shenzhen University. His research interests cover the synthesis, structure, properties and device of organic/polymeric optoelectronic materials.

1. Introduction

With the increasing demand for environmental friendly renewable energy, it is imperative to develop new photovoltaic (PV) technologies to meet the diverse market application needs.[1–20] Bulk-heterojunction (BHJ) organic solar cells (OSCs), as a prospective PV technology, have attracted a great deal of attention due to their unique advantages, including solution processibility, color-turnability, and easy fabrication into lightweight, large-area and flexible devices.[8,21–35] Thanks to material development and device innovation, BHJ OSCs have achieved rapid progress over the past three decades.[36–58] The device efficiencies of OSCs have increased explosively since the emergence of fused-ring small-molecule acceptors (SMAs) in 2015.[59–65] Among a myriad of nonfullerene SMAs, imides, acceptor–(π)–donor–(π)–acceptor (A–(π)–D–(π)–A)-type and A–DA$_1$D–A-type acceptors are the most popular systems due to their excellent device performance,[66–78] among which the most representative SMAs are ITIC[9] and Y6,[10] respectively. To date, nonfullerene SMA-based OSCs have achieved PCEs over 19%,[25,62–65,79–81] which has now reached the threshold of commercial application.

Typically, nonfullerene SMAs consist of a central core, two or more terminal acceptor units, and side chains that ensure sufficient solubility so that the molecules can be solution-processable.[9–12] By manipulating central cores or terminal acceptor units, the optoelectronic properties of the molecules can be finely tuned, but the only drawback is that manipulating these two parts is relatively time-consuming and complex as compared with modifying side chains.[72,82–85] Side-chain engineering is a direct, convenient and feasible method to optimize the chemical structures of molecules, then effectively regulate the absorption, energy levels, solubility, electron mobility, molecular interaction/aggregation, and ultimately promote the improvement of device efficiency.[72,82–85] On the other hand, side-chain engineering offers an intuitive method to probe the structure–property relationship of SMAs with a subtle structural change in side chains.[72,82–85] Basically, there are four main

avenues to modify the side chains (Fig. 1): (1) changing the length, branched alkyl chains, branching point, and position; (2) heteroatom substitution, such as O, S, Se, Si, F, Cl and so on; (3) employing different aromatic rings, including benzene, thiophene, selenophene, thieno[3,2-*b*]thiophene, diphenylamine, *etc.*; and (4) incorporating special functional groups into side chains, such as oligo(ethylene glycol) chains, siloxane-terminated side chains, urea and carboxylic acid groups. As a matter of fact, much effort has been devoted to amending the side chains of A–(π)–D–(π)–A-type acceptors and A–DA$_1$D–A-type acceptors, and the PCEs of OSCs based on SMAs have increased from 2% to 5% through optimizing the side chains.

There have been a great deal of review articles and accounts presenting the evolution of nonfullerene SMAs on different topics, including asymmetric SMAs,[18,86,87] isomerization strategy of SMAs,[37] end-capping engineering on SMAs,[88,89] and the influences of central cores on SMAs.[5,45,90–92] However, up to now, there is still no review or account that systematically summarizes the development of side-chain engineering on nonfullerene SMAs. In light of the recent important advances in side-chain engineering of SMAs, it is necessary to briefly review the influence of side chains on the physicochemical properties and cell efficiency of SMAs in recent years. In this article, we first present the recent progress of side-chain engineering in A–(π)–D–(π)–A-type nonfullerene SMAs and A–DA$_1$D–A-type nonfullerene SMAs. Then, some important examples that can enhance device performance *via* side-chain engineering will be highlighted. Finally, we will carefully discuss the future directions of side-chain engineering and provide a perspective for next generation SMAs.

2. Side-chain engineering of A–(π)–D–(π)–A-type SMAs

Since the invention of ITIC[9] (a typical A–D–A-type SMA) developed by Zhan and co-workers, SMAs with an A–D–A architecture

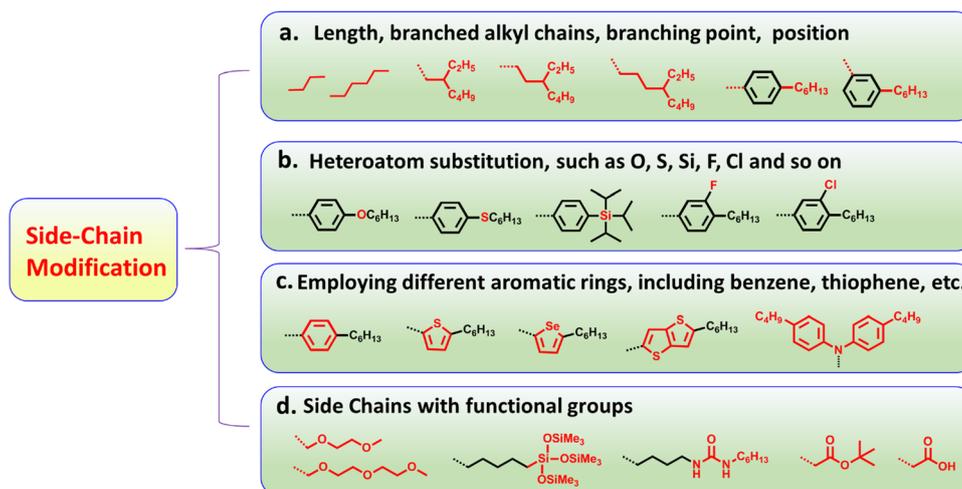

Fig. 1 The illustration of methods for modifying the side chains of organic semiconductor materials.
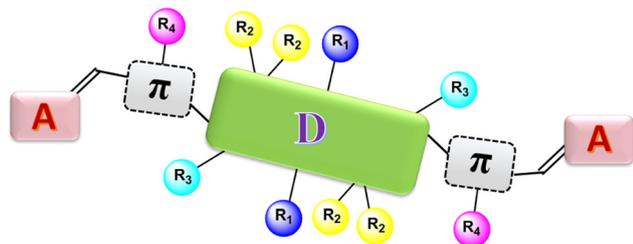
This journal is © The Royal Society of Chemistry 2023

Energy Environ. Sci., 2023, **16**, 2732–2758 | **2733**

Fig. 2 The illustration of avenues for modifying the side chains of A−π−D−π−A type SMAs.

have received considerable attention and made great breakthroughs.[93–97] In general, A–D–A-structured SMAs are made up of a central electron-donating core (D), multiple side chains and two terminal acceptor groups. Conjugated π bridges are sometimes employed to connect the central core and the two terminal units in A–D–A architecture SMAs, thus constructing A–π–D–π–A-structured SMAs. Manipulation of D, A, side chains and π bridges is a feasible way to enhance device efficiency. As shown in Fig. 2, there are typically four positions for altering the side chains of A–π–D–π–A-structured SMAs. Much effort has been devoted to modifying the side chains at these four positions, resulting in rapid progress in device efficiency.

2.1. Side-chain engineering of IDTT-based SMAs

As we know, ITIC is composed of a indacenodithieno[3,2-*b*]-thiophene (IDTT) unit flanked by four *para*-hexylphenyls and two end groups of 2-(3-oxo-2,3-dihydro-1*H*-inden-1-ylidene)malononitrile (INCN).[9] Modifying the side chains (R_1 in benzene, R_2 in cyclopentadiene, and R_3 in thieno[3,2-*b*]thiophene) in IDTT of ITIC can be a useful means to trim the molecular structures (Fig. 3), which in turn enables high cell efficiency.

Much effort was devoted to altering the side chains R_2 in ITIC. For example, Zhan and co-works developed a SMA of ITIC-Th by replacing 4-hexylphenyl in ITIC with 2-hexylthienyl.[93] In comparison with ITIC, ITIC-Th possesses enhanced intermolecular interactions ascribed to the presence of more polarized S atom. When ITIC-Th is blended with a small band-gap polymer donor PTB7-Th, it can afford a device efficiency of 8.7%, and a higher PCE of 9.6% can be obtained after pairing it with wide-band-gap donor PDBT-T1 (Table 1). Similarly, Yang *et al.* replaced the hexylphenyl in ITCPTC with hexylthienyl and hexylselenyl to get two SMAs, namely, ITCPTC-Se and ITCPTC-Th.[94] ITCPTC-Th and ITCPTC-Se show much higher absorption coefficients than ITCPTC. Compared to ITCPTC-Th, ITCPTC-Se exhibits

slightly redshifted absorption and upshifted energy levels ascribed to the σ-inductive effect of Se, but weaker crystallinity duo to the larger atomic radius of Se. OSC based ITCPTC-Th yielded a PCE of 10.61% along with an FF of 0.727, which are superior to those of ITCPTC-Se based one (PCE = 9.02%; FF = 0.683) (Fig. 4). Parallelly, Li *et al.* changed the alkyl substitution position on ITIC with 4-hexylphenyl substitution to 3-hexylphenyl substitution to create *m*-ITIC.[95] Compared to ITIC, *m*-ITIC shows slightly blue-shifted absorption in solution but redshifted absorption in films, indicating its reinforced molecular parking. The J61:*m*-ITIC device presents a better PCE of 11.77% as compared to the ITIC-based device (10.57%). Moreover, the PCE remains over 8.00% when the thickness of the active layer is 350 nm.

The alkoxyl chains have been widely utilized to survey their impact on device efficiency. For instance, Zou *et al.* adopted a long alkoxyl chain to replace the alkyl chain on *m*-ITIC to obtain *m*-ITIC-OR, which exhibited relatively blue-shifted absorption spectra and a downshifted LUMO value relative to *m*-ITIC.[96] The device based on *m*-ITIC-OR achieved a decent efficiency of 9.30%. In addition, Chen *et al.* developed two SMAs of IDTT-OBH and IDTT-BH with alkoxyl chains.[97] Compared with IDTT-BH, IDTT-OBH showed slightly redshifted absorption in solution but blue-shifted absorption in films. When blended with J71 and PDCBT, IDTT-BH based devices present better morphology, and thus higher PCEs than IDTT-OBH based devices; while when blended with PBDB-T, the device based on IDTT-OBH shows higher PCE than the IDTT-BH-based device. Lee and co-workers also studied the influence of alkoxyl chains on photoelectric properties and cell efficiency.[98] Compared to *m*-ITIC-H, *m*-ITIC-O-EH and *m*-ITIC-O-H with alkoxyl side chains exhibit increased surface energy, and *m*-ITIC-O-EH with branched alkoxyl chains shows weaker aggregation properties in comparison to *m*-ITIC-O-H with linear alkoxyl side chains. The device based on *m*-ITIC-O-EH showed good active layer-thickness tolerance, and a high PCE of 9.68% could be achieved by the printing process in air. Gao *et al.* further surveyed the impacts of alkoxy chains and fluorination on cell efficiency.[99] pO-ITIC with 4-hexyloxyphenyl and mO-ITIC with 3-hexyloxyphenyl demonstrated lower band gaps, enhanced absorption ability and higher LUMO energy levels relative to those of FpO-ITIC with 3-fluorine-4-hexyloxy-phenyl. As results, PTB7-Th:mO-ITIC and PTB7-Th:pO-ITIC devices present very similar PCEs of 7.51% and 7.33%, which are higher than those of device based on FpO-ITIC (6.17%).

In addition to O atoms, S atoms are often inserted into alkyl chains to optimize the molecular properties. Bo and co-workers developed three SMAs (ITIC-SC2C6, ITIC-SC8, and ITIC-SC6), changed the alkylphenyl on ITIC to alkylthiophenyl, and investigated the influence of branched chains and side-chain length on photovoltaic performance.[100] ITIC-SC2C6 with branched 2-ethylhexyl chains showed a longer molecular packing distance in comparison to linear side chains molecules (ITIC-SC8 and ITIC-SC6), and ITIC-SC2C6 presented slightly larger bandgaps and downshifted energy levels. The PBDB-ST:ITIC-SC2C6 device gave the best PCE of 9.16% due to well-performing morphology.
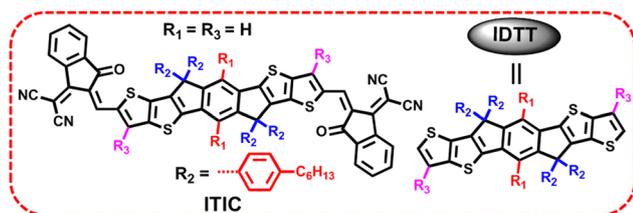

Fig. 3 The chemical structures of ITIC and IDTT.

2734 | *Energy Environ. Sci.*, 2023, **16**, 2732–2758

This journal is © The Royal Society of Chemistry 2023

Table 1 Optical, electrochemical and photovoltaic data of IDTT-based SMAs with different side chains

SMA	$E_g^{opt\ a}$ (eV)	HOMO[b]/LUMO[b] (eV)	Donor	V_{OC} (V)	J_{SC} (mA cm^{-2})	FF (%)	PCE (%)	Ref.
ITIC	1.59	−5.48/−3.83	PTB7-Th	0.81	14.21	0.591	6.8	9
ITIC-Th	1.60	−5.66/−3.93	PDBT-T1	0.88	16.24	0.671	9.6	93
ITCPTC-Th	1.60	−5.66/−3.93	PBDB-T	0.856	17.05	0.727	10.61	94
ITCPTC-Se	1.59	−5.66/−3.93	PBDB-T	0.869	15.20	0.683	9.02	94
m-ITIC	1.58	−5.52/−3.82	J61	0.912	18.31	0.7055	11.77	95
m-ITIC-OR	1.65	−5.65/−3.97	HFQx-T	0.90	16.15	0.64	9.13	96
IDTT-BH	1.54	−5.42/−3.86	J71	0.90	17.77	0.691	11.05	97
IDTT-OBH	1.57	−5.41/−3.86	PBDB-T	0.87	17.46	0.720	10.93	97
m-ITIC-H	1.61	−5.21/−3.60	PBDB-T	0.85	15.09	0.67	8.54	98
m-ITIC-O-H	1.60	−5.25/−3.65	PBDB-T	0.85	15.99	0.70	9.55	98
m-ITIC-O-EH	1.62	−5.25/−3.63	PBDB-T	0.88	15.88	0.68	9.77	98
pO-ITIC	1.61	−5.49/−3.71	PTB7-Th	0.80	14.79	0.591	7.51	99
mO-ITIC	1.63	−5.50/−3.74	PTB7-Th	0.80	14.19	0.601	7.33	99
FpO-ITIC	1.64	−5.61/−3.72	PTB7-Th	0.78	12.99	0.567	6.17	99
ITIC-SC6	—	−5.68/−3.91	PBDB-ST	0.90	13.92	0.58	7.27	100
ITIC-SC8	—	−5.70/−3.90	PBDB-ST	0.90	14.43	0.60	7.79	100
ITIC-SC2C6	—	−5.74/−3.86	PBDB-ST	0.92	15.81	0.63	9.16	100
o-F-ITIC	1.58	−5.66/−3.94	PBDB-T	0.918	18.07	0.6697	11.11	101
m-F-ITIC	1.62	−5.69/−3.96	PBDB-T	0.883	15.80	0.6379	8.9	101
C8-ITIC	—	−5.63/−3.91	PFBDB-T	0.94	19.6	0.72	13.2	103
IDTT-C6-TIC	1.60	−5.55/−3.99	PBT1-C	0.85	17.0	0.667	10.0	104
IDTT-C8-TIC	1.59	−5.64/−3.97	PBT1-C	0.88	20.3	0.746	13.7	104
IDTT-C10-TIC	1.61	−5.71/−3.91	PBT1-C	0.98	18.1	0.713	12.7	104
ITIC-OE	1.57	−5.67/−4.03	PBDB-T	0.85	14.8	0.67	8.5	105
ITIC-OEG	1.54	−5.39/−3.99	PPDT2FBT	0.90	3.56	0.49	1.58	106
ITC6-IC	1.60	−5.73/−3.92	PBDB-T	0.97	16.41	0.73	11.61	107
ITIC	1.58	−5.68/−4.01	PBDB-T	0.91	16.27	0.69	10.21	107
IT-4F	1.51	−5.74/−4.26	PM6	0.85	20.02	0.7522	12.80	108
IM-4F	1.46	−5.69/−4.19	PM6	0.88	22.12	0.7279	14.17	108
IOM-4F	1.48	−5.72/−4.27	PM6	0.86	21.66	0.7200	13.41	108
IMC6-4F	1.49	−5.71/−3.94	PM6	0.90	22.29	0.7759	15.57	109

[a] Calculated from $E_g^{opt} = 1240/\lambda_{onset}$. [b] Calculated from CV curves.

Incorporation of an F atom into the phenyl side chains of ITIC can also be a useful for promoting cell efficiency. Yang *et al.* reported two acceptors, *m*-F-ITIC and *o*-F-ITIC, with different fluorination sites; in comparison with ITIC, *m*-F-ITIC with meta-alkyl substitution and *o*-F-ITIC with ortho-alkyl substitution show gradually blue-shifted absorption, downshifted energy levels, and weaker crystallinity.[101] OSCs based on *o*-F-ITIC yielded a higher efficiency of 11.11% compared with *m*-F-ITIC-based ones due to the closer donor–acceptor interaction in the *o*-F-ITIC: PBDB-T blend. The same molecules and similar conclusions were also reported by Xin *et al.*, that is, the device based on *m*F-ITIC presented a higher PCE of 9.50% with enhanced thermal stability relative to that of the *o*F-ITIC-based device.[102]

Via alkyl side-chain substitution, Heeney *et al.* obtained a new SMA of C8-ITIC with octyl groups. C8-ITIC delivered much redshifted absorption, higher absorption coefficients and enhanced crystallinity in comparison to ITIC.[103] The PFBDB-T:C8-ITIC device showed a decent PCE of 13.2%, accompanied with a low energy loss of 0.60 eV, which are superior to those of the ITIC-based device. Additionally, Sun and co-workers investigated the influence of alkyl side-chain length on molecular packing behaviors.[104] IDTT-C6-TIC with hexyl chains showed a strong molecular π–π stacking mode, and IDTT-C8-TIC with octyl chains exhibited and intermixed packing mode, whereas IDTT-C10-TIC with decyl side chains showed a non-stacking mode. Eventually, PBT1-C:IDTT-C8-TIC OSCs afforded the best PCE of 13.7% with low structural disorder and non-radiative recombination loss among the three devices.

Exploiting SMAs with high dielectric constants (ε_r) is a promising method to reduce the exciton binding energy and boost device efficiency. Huang *et al.* replaced the hexyl alkyl side chains on ITIC with oligoethylene oxide (OE) side chains to get ITIC-OE.[105] Compared to ITIC, ITIC-OE showed slightly blue-shifted absorption in solution but redshifted absorption in films, a decreased surface energy, and a larger ε_r of 9.4. The devices based on ITIC-OE delivered a lower efficiency of 8.5% due to the weaker crystallinity of ITIC-OE and smaller micro-phase separation, as compared with ITIC-based devices. Also, Woo and co-workers empolyed oligoethyleneglycol (OEG) groups to replace the hexyl alkyl side chains in ITIC to afford ITIC-OEG.[106] ITIC-OEG exhibited distinctly redshifted absorption, upshifted energy levels, reinforced molecular parking, and a greatly enhanced dielectric constant in comparison to ITIC. Ascribed to the high hydrophilic properties of OEG chains, ITIC-OEG presented poor miscibility with PPDT2FBT, and thus the PPDT2FBT:ITIC-OEG device exhibited a PCE of only 1.58%.

Different from modifying R_2, manipulation of R_1 and R_3 in IDTT-based SMAs received less attention, and most of the related works were reported by Tang' group. In 2018, they incorporated two hexyl side chains into the β position of peripheral thiophene in the central core of ITIC for conformation locking to obtain a new SMA of ITC6-IC (Fig. 5).[107] According to density functional theory (DFT) calculations, ITC6-IC showed a highly unified and planar configuration because of the steric hindrance impact of the hexyl moiety. In comparison with ITIC,

This journal is © The Royal Society of Chemistry 2023

Energy Environ. Sci., 2023, **16**, 2732–2758 | **2735**

Fig. 4 Chemical structures of IDTT-based SMAs with different side chains.

Fig. 5 (a) The chemical structures of ITIC and ITC6-IC; (b) possible rotamers at 0° and 180° in TTC6-IC and TT-IC; (c) potential energy surface curves of TT-IC and TTC6-IC; (d) absorption spectra of ITC6-IC and ITIC; (d) CV curves of ITC6-IC and ITIC; (f) J–V curves of PBDB-T:ITC6-IC device without and with thermal annealing and PBDB-T:IT-IC device. Adapted with permission.[107] Copyright 2018, Wiley-VCH.

2736 | Energy Environ. Sci., 2023, 16, 2732–2758

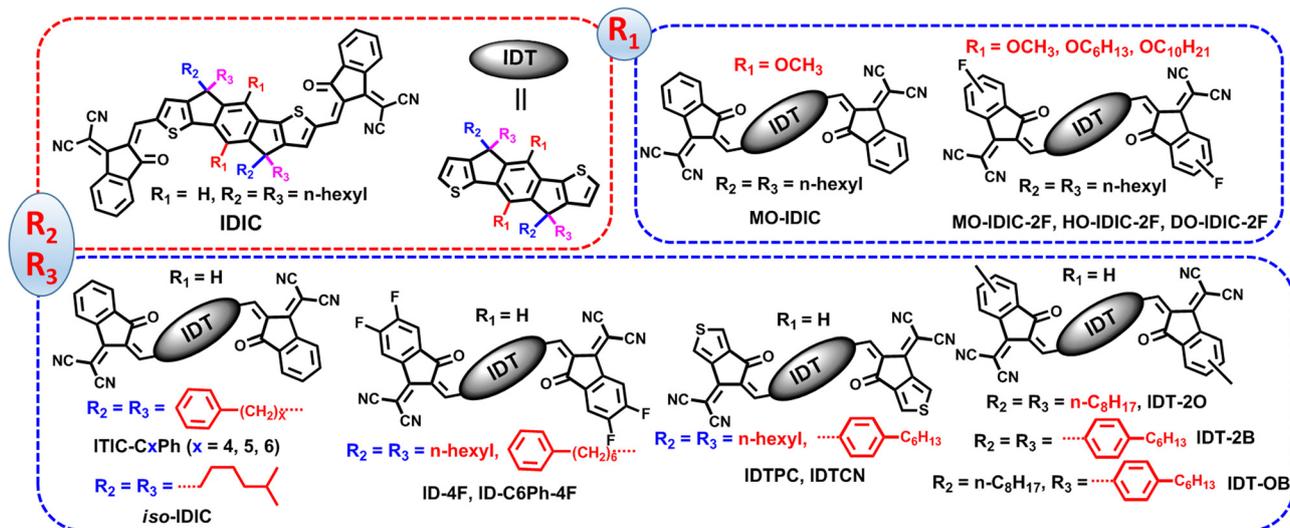This journal is © The Royal Society of Chemistry 2023

Fig. 6 Chemical structures of IDT-based A−D−A type SMAs with different side chains.

ITC6-IC exhibited redshifted absorption and higher absorption coefficients in solution due to the planar structure caused by conformation locking, but an upshifted LUMO value and blue-shifted absorption in films, which resulted from the weak electron-donating properties of the hexyl moiety. After pairing ITIC and ITC6-IC with PBDB-T, the device based on ITC6-IC afforded a device efficiency of 11.61%, accompanied with a high V_{OC} of 0.97 V, performing better than the ITIC-based device (10.21%). Later, the same group focused on the central benzene moiety in IDTT-based SMAs and developed two SMAs (IOM-4F and IM-4F) by replacing H atoms with weak electron-rich methoxy or methyl units.[108] Compared to IT-4F, IOM-4F and IM-4F showed redshifted absorption due to the electron-donating ability of methyl and methoxy groups. In addition, IM-4F exhibited obviously upshifted molecular energy levels relative to those of IT-4F, whereas IOM-4F presented higher crystallinity and rigid conformations due to S···O noncovalent interactions. Together with PM6, the devices based on PM6:IM-4F and PM6:IOM-4F achieved simultaneously enhanced J_{SC}s and V_{OC}s with PCEs of 14.17% and 13.41%, respectively. The higher V_{OC} in IOM-4F and IM-4F devices is ascribed to the reduced nonradiative recombination loss, as confirmed by energy loss experiments. Furthermore, they employed a strategy of combining the weak electron-donating methyl substitution in the central phenyl unit and outer thiophene β position alkyl conformation locking to develop IMC6-4F.[109] IMC6-4F presented slightly blue-shifted absorption spectra and downshifted HOMO values compared with IM-4F. Finally, PM6:IMC6-4F cells delivered a good efficiency of 15.57%, with an outstanding FF of 0.7759, a J_{SC} of 22.29 mA cm^{-2} and a decent V_{OC} of 0.90 V.

2.2. Side-chain engineering of IDT-based SMAs

Indacenodithiophene (IDT), as an earlier developed electron-donating unit, has shown great potential in constructing high-efficiency SMAs and polymer acceptors.[110–113] In this part, we will introduce side-chain engineering of IDT-based SMAs from

two aspects: (a) side-chain engineering of IDT-based A–D–A type SMAs and (b) side-chain engineering of IDT-based A–π–D–π–A type SMAs.

2.2.1 Side-chain engineering of IDT-based A–D–A type SMAs. IDIC, a star IDT-based SMA, contains a IDT core and two INCNs. Compared with ITIC, the positions of the modifiable side chain in IDIC are same, namely, R_1 in benzene, R_2 (or R_3) in cyclopentadiene.

Li and co-workers introduced two methoxy groups into benzene of IDIC to afford MO-IDIC.[112] The synthetic route of MO-IDIC was simplified, and the molecule displayed slightly red-shifted absorption but an up-shifted LUMO value relative to IDIC. The OSC based PTQ10:MO-IDIC yielded a PCE of 11.16% (Fig. 6). To further improve the device performance, they replaced INCN in IDIC with monofluorinated INCN and systematically optimized the length of alkoxy side chains on the benzene ring, and finally obtained four new SMAs (MO-IDIC-2F, HO-IDIC-2F and DO-IDIC-2F).[113] As the length of the alkoxy side chain increased, the three SMAs (from MO-IDIC-2F, HO-IDIC-2F to DO-IDIC-2F) demonstrated gradually red-shifted absorption spectra, elevated HOMO and LUMO levels, an improved molecular order and molecular self-assembly. Consequently, the PM6:DO-IDIC-2F device with longest chains realized the highest PCE of 13.02% along with the best J_{SC} of 19.63 mA cm^{-2} among the three SMA-based devices (Table 2).

Yang and co-workers compared the effect of aryl and alkyl chains in cyclopentadiene on molecular orientation and device efficiency.[114] GIWAXS experiments indicated that IDTCN with 4-hexylphenyl shows an unoriented molecular arrangement, while obvious face-to-face molecular orientation was observed in IDTPC with n-hexyl chains. The IDTPC-based device yielded higher J_{SC} and FF, thereby better PCE (12.2%), as compared to IDTCN-based ones. The enhanced J_{SC} and FF mainly attribute to better molecular π–π packing and promoted charge mobility.

Bo and co-workers simultaneously introduced A and B onto the same sp^3-hybridized carbon atom of cyclopentadiene to

This journal is © The Royal Society of Chemistry 2023

Energy Environ. Sci., 2023, **16**, 2732–2758 | **2737**

Table 2 Optical, electrochemical and photovoltaic data of IDT-based A–D–A type SMAs with different side chains

SMA	$E_g^{opt\ a}$ (eV)	HOMO^b/LUMO^b (eV)	Donor	V_{OC} (V)	J_{SC} (mA cm^{-2})	FF (%)	PCE (%)	Ref.
IDIC	1.62	−5.69/−3.91	PDBT-T1	0.89	15.05	0.65	8.71	111
MO-IDIC	1.60	−5.69/−3.89	PTQ-10	0.969	16.92	0.681	11.16	112
IDIC-2F	1.57	−5.75/−3.95	PM6	0.846	17.95	0.758	11.52	112
MO-IDIC-2F	1.55	−5.80/−3.93	PM6	0.843	18.92	0.767	12.23	113
HO-IDIC-2F	1.55	−5.81/−3.91	PM6	0.863	19.05	0.763	12.53	113
DO-IDIC-2F	1.54	−5.79/−3.98	PM6	0.864	19.63	0.765	13.02	113
IDTCN	1.67	−5.91/−3.84	PTQ10	0.98	13.9	0.54	7.4	114
IDTPC	1.52	−5.98/−3.98	PTQ10	0.93	17.5	0.746	12.2	114
IDT-2B	1.73	−5.80/−3.84	PBDB-T	0.89	13.3	0.539	6.42	115
IDT-OB	1.66	−5.77/−3.87	PBDB-T	0.88	16.18	0.711	10.12	115
IDT-2O	1.64	−5.73/−3.85	PBDB-T	0.86	15.64	0.723	9.68	115
IDIC-PhC6	1.71	−5.72/−3.86	PBDB-T	0.869	12.2	0.579	6.14	116
IDIC	1.63	−5.70/−3.92	PM6	0.947	18.17	0.6988	12.02	116
IDIC-C4Ph	1.62	−5.70/−3.93	PM6	0.941	19.06	0.7832	14.04	117
IDIC-C5Ph	1.66	−5.76/−3.89	PM6	0.948	19.19	0.8002	14.56	117
IDIC-C6Ph	1.65	−5.84/−3.86	PM6	0.946	17.29	0.7683	12.57	117
iso-IDIC	—	−5.84/−3.84	PM6	0.961	18.91	0.7445	13.53	118
IDIC	—	−5.83/−3.87	PM6	0.963	17.94	0.7160	12.37	118

^{a} Calculated from $E_g^{opt} = 1240/\lambda_{onset}$. ^{b} Calculated from CV curves.

develop a SMA of IDT-OB with asymmetric chains.[115] In comparison with two sysmetric counterparts (IDT-2O and IDT-2B), IDT-OB exhibited improved solubility, closer molecular packing and more favorable domain size after blending with PBDB-T. Finally, the device based on IDT-OB delivered the best efficiency of 10.12%.

Li and co-workers found that IDIC shows strong crystallization and face-on orientations, and IDIC-PhC6 with 4-hexyl-phenyl exhibits weak crystallization but good solubility. To achive a balance between molecular aggregation and miscibility, they introduced a bulky phenyl onto the the tail of *n*-butyl and reported an SMA, IDIC-C4Ph.[116] IDIC-C4Ph inherits the face-on orientation features of IDIC and shows moderate crystallinity as compared with IDIC and IDIC-PhC6 (Fig. 7). After blending with star polymer donor PM6, an ideal morphology with proper phase separation and good molecular crystallization characteristics were observed in the IDIC-C4Ph-based blend, which led to the highest efficiency of 14.02% as well as an outstanding FF of 0.7832 in the PM6:IDIC-C4Ph device. Then, they trimmed the length of the alkyl chains (from C4 to C6) and obtained three SMAs, namely, IDIC-C4Ph, IDIC-C5Ph, and IDIC-C6Ph.[117] The single crystal results showed that a two charge-transport channel was observed in IDIC-C5Ph, contributing to the electron hopping. As the alkyl chain continue to grow, disordered molecular orientations are seen in IDIC-C6Ph. The cells based on IDIC-C5Ph realized an efficiency of 14.56% along with an impressive FF of 0.8002, outperforming those of the devices based on IDIC-C4Ph (PCE = 13.94%; FF = 0.7805) and IDIC-C6Ph (PCE = 12.57%; FF = 0.7683). Finally, the same group focused on the isomerization of alkyl chains. They replaced the linear alkyl chains in IDIC with a branched one containing an isopropyl terminal to obtain an acceptor, iso-IDIC.[118] This strategy endows iso-IDIC with slightly reduced crystallinity but comparable optical and electrochemistry characteristics relative to those of IDIC. Consequently, the iso-IDIC-based device realizes a better efficiency of 13.50% because of a morphology with decreased aggregation.

2.2.2 Side-chain engineering of IDT-based A–π–D–π–A type SMAs. π spacers are usually linked between the central core and two terminal units to further broaden molecular absorption spectra. The commonly used π spacers include thiophene, benzene, thieno[3,4-*b*]thiophene and so on. For IDT-based A–π–D–π–A type SMAs, the main way to modify side chains is on the π spacers.

In 2015, Zhan and co-workers reported an A–π–D–π–A type acceptor (IEIC) with a side chain at the inner position of the π spacer (Fig. 8), and the device based on PTB7-TH:IEIC yielded a PCE of 6.31% (Table 3), which represented the best result for SMA-based OSCs at the time.[119] Then, Hou and co-workers replaced 2-ethylhexyl with an alkoxy side chain to obtain a low bandgap SMA of IEICO. IEICO showed an obvious smaller optical bandgap of 1.34 eV and enhanced molecular stacking relative to IEIC.[120] In consequence, the IEICO-based device delivered a higher PCE of 8.4% compared to the IEIC-based one due to the significantly improved J_{SC} and FF. Furthermore, Bazan *et al.* employed an alkyl–alkoxy-combination strategy to develop two asymmetric new acceptors (*p*-IO1 and *o*-IO1) with monoalkoxy chains.[121] Compared with bisalkoxy counterparts, the monoalkoxy ones showed blue-shifted absorption spectra and higher LUMO values. Together with the polymer donor PTB7-Th, the *o*-IO1-based device realizes a higher PCE of 13.2%, which is mainly ascribed to the high J_{SC} and low energy loss.

Bo and co-workers investigate the impact of the outer side chains of the π spacer in IDT-based A–π–D–π–A-type acceptors on molecular interaction and cell performance. Three SMAs with different chains (alkoxyl, alkylthio, and alkyl) were synthesized.[122] Compared with IDTCN-C and IDTCN-S, IDTCN-O exhibits a higher LUMO level and stronger molecular packing, resulting in enhanced V_{OC} and FF, and thereby a better PCE of 13.28% in PBDB-T:IDTCN-O as the cast device. The same group demonstrated that the introduction of alkoxy chains on the outermost thiophenes of IDT in IDT-based A–π–D–π–A-type

2738 | *Energy Environ. Sci.*, 2023, **16**, 2732–2758

This journal is © The Royal Society of Chemistry 2023

Fig. 7 (a) GIWAXS scattering patterns of IDIC-C4Ph, IDIC, and IDIC-PhC6; (b) the schematic diagram of molecular stacking in pure IDIC-C4Ph, IDIC, and IDIC-PhC6 films and their corresponding PM6:acceptor blends. Adapted with permission.[116] Copyright 2019, Wiley-VCH.

Fig. 8 Chemical structures of IDT-based A−π−D−π−A type SMAs with different side chains.

This journal is © The Royal Society of Chemistry 2023

Energy Environ. Sci., 2023, **16**, 2732–2758 | **2739**

Table 3 Optical, electrochemical and photovoltaic data of IDT-based A−π−D−π−A type SMAs with different side chains

SMA	$E_g^{opt \, a}$ (eV)	HOMO[b]/LUMO[b] (eV)	Donor	V_{OC} (V)	J_{SC} (mA cm^{-2})	FF (%)	PCE (%)	Ref.
IEIC	1.57	−5.42/−3.82	PTB7-Th	0.97	13.5	0.48	6.31	119
IEICO	1.34	−5.32/−3.95	PBDTTT-E-T	0.82	17.7	0.58	8.4	120
p-IO1	1.34	−5.46/−4.13	PTB7-Th	0.78	22.3	0.62	10.8	121
p-IO2	1.28	−5.44/−4.15	PTB7-Th	0.74	26.3	0.67	13.1	121
o-IO1	1.24	−5.44/−4.19	PTB7-Th	0.70	23.0	0.67	10.8	121
o-IO2	1.20	−5.41/−4.21	PTB7-Th	0.68	21.8	0.63	9.3	121
IDTCN-C	1.48	−5.59/−3.92	PBDB-T	0.84	20.33	0.696	11.92	122
IDTCN-O	1.53	−5.54/−3.80	PBDB-T	0.91	19.96	0.732	13.28	122
IDTCN-S	1.48	−5.57/−3.90	PBDB-T	0.85	19.04	0.657	10.60	122
IDTT2F	1.46	−5.57/−4.03	PBDB-T	0.81	18.51	0.59	8.85	123
IDTOT2F	1.44	−5.54/−3.94	PBDB-T	0.85	20.87	0.72	12.79	123
IDT-T$_o$FIC	1.50	−5.55/−3.86	PBDB-T	0.88	17.79	0.71	11.09	124
IDT-T$_i$FIC	1.41	−5.57/−4.05	PBDB-T	0.86	16.97	0.65	9.46	124
IDTC	1.51	−5.57/−3.96	PBDB-T	0.917	16.56	0.6161	9.35	125
IDTO	1.53	−5.52/−3.84	PBDB-T	0.943	16.25	0.6541	10.02	125
i-IE-4F	1.51	−5.43/−3.79	J52	0.84	18.34	0.4757	7.34	126
i-IESi-4F	1.51	−5.50/−3.71	PBZ-2Si	0.87	22.55	0.7403	14.54	126
IDT-BC6	1.75	−5.55/−3.82	PBDB-T	0.92	5.63	0.44	2.3	127
IDT-BOC6	1.63	−5.51/−3.78	PBDB-T	1.01	17.52	0.54	9.60	127

[a] Calculated from $E_g^{opt} = 1240/\lambda_{onset}$. [b] Calculated from CV curves.

acceptors is also a means to improve molecular packing and device efficiency.[123] In addition, they reported two regioisomeric SMAs, namely, IDT-T-iFIC with inner 5-hexylthienyl chains and IDT-T-oFIC with outer 5-hexylthienyl chains.[124] In comparison with IDT-TiFIC, the IDT-T$_o$FIC-based device delivered an enhanced PCE of 11.09%, which is mainly due to the better morphology and lower energy loss. This isomeric method was also reported by employing a 2-ethylhexyl carboxylate group, but a different trend in PCE was observed.

When the termial unit INCNs of IEIC and IEICO were replaced with thiophene-fused end groups, two new SMAs, IDTC and IDTO, were acquired.[125] These two SMAs exhibited completely different properties from those of IEIC and IEICO. IDTO with alkoxy chains displayed slightly blue-shifted absorption and an upshifted LUMO value relative to those of IDTC. The IDTO-based device showed an efficiency of 10.02%, higher than that of the IDTC-based one (PCE = 9.35%).

Chen and co-workers first empolyed siloxane-terminated chains to develop an SMA, i-IESi-4F. The siloxane-terminated units endows i-IESi-4F with good solubility and low surface energy.[126] When blended with polymer donors PBZ-2Si or J52, i-IESi-4F shows better misbility than i-IE-4F with ackyl chains. In OSCs, i-IESi-4F shows a significantly higher PCE of 14.54% compared to i-IE-4F (7.34%).

Employing benzene as π spacers to construct high-performance SMAs has been proven to be a successful way. Bo and co-workers developed two electron acceptors (IDT-BOC6 and IDT-BC6) with benzene as π spacers; the difference between the two SMAs was that the side chains on the benzene were different: for IDT-BC6, it was n-hexyl, and for IDT-BOC6, it was hexyloxy.[127] The conformation locking of S···O and O···H endows IDT-BOC6 with a more planar molecular structure, a narrower bandgap, emhanced charge mobility, lower energy loss compared with IDT-BC6. In OSCs with PBDB-T as a donor, IDT-BOC6 realized a PCE of 9.6%, obviously better than the IDT-BC6-based cell (2.3%).

2.3. Side-chain engineering of BDT-based SMAs

Benzo[1,2-b:4,5-b′]dithiophene (BDT) as a star scaffold has been widely applied to synthetize organic photovoltaic materials, such as small-molecular donors, polymer donors and SMAs, due to its excellent charge transport properties.[128–133]

In 2017, Zhan et al. introduced 2D thiophene conjugated side chains onto an SMA, ITIC1 (the isomer of ITIC), to construct nonfullerene acceptor ITIC2 (Fig. 9).[131] Attributed to enhanced intramolecular conjugation and intermolecular interaction, ITIC2 presents red-shifted and enhanced absorption, slightly elevated HOMO/LUMO values, and improved charge mobility compared to ITIC1. The device based on ITIC2 exhibited a much better efficiency of 11.0% compared to the ITIC1-based device (8.54%). Then, Chen et al. introduced S atoms onto the 2D side chains and synthesized ITIC-S. Compared with ITIC2, ITIC-S showed slightly blue-shifted absorption, a reduced LUMO value, a higher absorption coefficient and electron mobility, and decreased crystallinity.[132] The PBDB-T-SF:ITIC-S-based device displayed a good efficiency PCE of 11.6% (Table 4). Subsequently, they introduced F atoms into 2D thiophene chains and synthesized ITIC-SF. The absorption of ITIC-SF was further blue-shifted and the energy level was further reduced.[133] Meanwhile, the absorption coefficient and crystallinity were increased. Finally, the device based on ITIC-SF displayed a decent efficiency of 12.1%. Furthermore, they replaced the benzene-fused end group with a thiophene-fused end group, and synthesized BDTSF-IC and BDTCH-IC.[134] Compared with BDTCH-IC, BDTSF-IC presents weaker crystallinity, which may be beneficial for forming favorable interpenetrating networks when blended with polymer donors. The PM6:BDTSF-IC device delivered an efficiency of 13.10%. In addition, Wang et al. adopted a 2D halogenated thiophene chain strategy and synthesized three nonfullerene SMAs, namely, ClBDT-4Cl FBDT-4Cl, and HBDT-4Cl.[135] Compared with non-halogenated HBDT-4Cl, ClBDT-4Cl and FBDT-4Cl
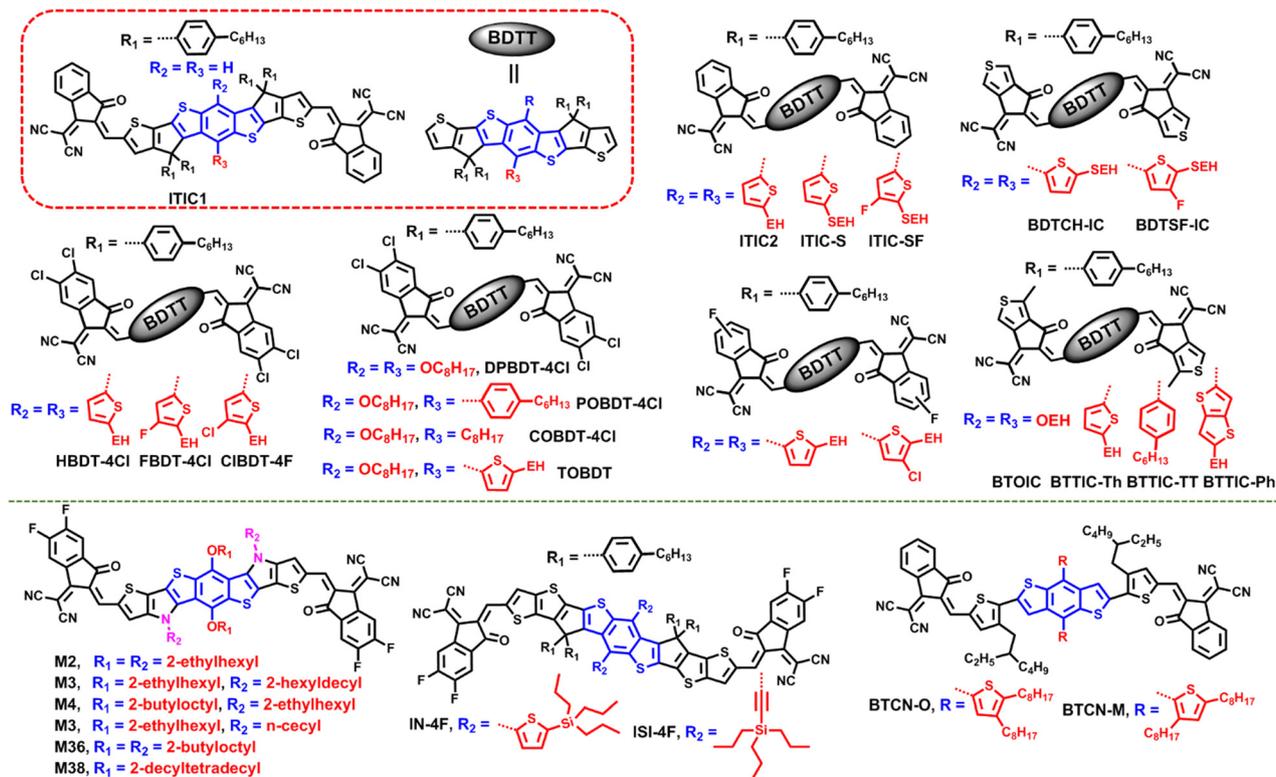
2740 | Energy Environ. Sci., 2023, **16**, 2732–2758

This journal is © The Royal Society of Chemistry 2023

Fig. 9 Chemical structures of BDT-based SMAs with different side chains.

Table 4 Optical, electrochemical and photovoltaic data of BDT-based SMAs with different side chains

SMA	$E_g^{opt\ a}$ (eV)	HOMO^b/LUMO^b (eV)	Donor	V_{OC} (V)	J_{SC} (mA cm^{-2})	FF	PCE%	Ref.
ITIC1	1.55	−5.48/−3.84	FTAZ	0.921	16.45	0.564	8.54	131
ITIC2	1.53	−5.43/−3.80	FTAZ	0.925	18.88	0.630	11.0	131
ITIC-S	1.55	−5.50/−3.86	PBDB-T-SF	1.06	16.43	0.668	11.6	132
ITIC-SF	1.58	−5.57/−3.92	PBDB-T-SF	1.04	16.85	0.686	12.1	133
BDTCH-IC	1.50	−5.51/−3.89	PM6	0.96	17.11	0.636	10.51	134
BDTSF-IC	1.56	−5.58/−3.93	PM6	0.90	20.36	0.7148	13.10	134
HBDT-4Cl	1.43	−5.67/−3.90	PM6	0.898	17.79	0.6476	10.35	135
FBDT-4Cl	1.45	−5.70/−3.91	PM6	0.888	19.83	0.7019	12.36	135
ClBDT-4Cl	1.44	−5.72/−3.92	PM6	0.879	19.02	0.6971	11.65	135
BTC-2F	1.53	−5.64/−3.91	PM6	0.92	20.3	0.693	12.9	136
BTH-2F	1.50	−5.59/−3.91	PM6	0.92	19.5	0.631	11.3	136
BTTIC-Th	1.467	−5.49/−3.90	PBDB-T	0.902	19.45	0.736	12.91	137
BTTIC-TT	1.474	−5.54/−3.80	PBDB-T	0.924	19.61	0.742	13.44	137
BTTIC-Ph	1.455	−5.48/−3.78	PBDB-T	0.930	16.47	0.597	9.14	137
BTOIC	1.39	−5.42/−3.94	PBDB-T	0.862	18.60	0.684	10.96	138
TOBDT	1.41	−5.56/−3.97	PM6	0.89	18.7	0.68	11.3	139
DPBDT-4Cl	1.41	−5.62/−3.94	PM6	0.90	19.2	0.66	11.4	140
POBDT-4Cl	1.39	−5.58/−3.97	PM6	0.88	21.0	0.68	12.6	140
COBDT-4Cl	1.39	−5.57/−3.98	PM6	0.87	21.8	0.71	13.5	141
IN-4F	1.38	−5.56/−3.99	PM6	0.870	21.8	0.692	13.0	141
ISI-4F	1.43	−5.65/−4.01	PM6	0.878	22.8	0.622	12.5	141
BTCN-O	1.53	−5.59/−3.95	PBDB-T	0.95	5.03	0.34	1.62	142
BTCN-M	1.63	−5.69/−3.95	PBDB-T	0.98	12.03	0.50	5.89	142
M2	1.39	−5.60/−3.96	PM6	0.88	19.76	0.6384	11.26	143
M4	1.38	−5.61/−3.97	PM6	0.88	23.44	0.7152	14.75	143
M36	1.39	−5.62/−3.95	PM6	0.90	24.63	0.7209	16.00	144
M38	1.47	−5.65/−3.93	PM6	0.87	18.28	0.5574	8.89	144
M3	1.41	−5.60/−3.85	PM6	0.96	11.34	0.5196	5.67	145
M32	1.41	−5.69/−3.84	PM6	0.91	24.03	0.7622	16.66	145

^{a} Calculated from $E_g^{opt} = 1240/\lambda_{onset}$. ^{b} Calculated from CV curves.

This journal is © The Royal Society of Chemistry 2023

Energy Environ. Sci., 2023, **16**, 2732–2758 | **2741**

with substituted Cl atoms and F atoms showed slightly blue-shifted absorption, enhanced light absorption ability and reduced energy levels, but reinforced molecular packing. ClBDT-4Cl- and FBDT-4Cl-based blends displayed a PCE of 11.65% and 12.36%, respectively, performing better than the HBDT-4Cl-based one (10.35%). Similar work was also reported by Zhang's team.[136]

In 2019, Yang et al. investigated the impact of the 2D conjugated moiety on photovoltaic performance and synthesized BTTIC-Th with a thiophene moiety, BTTIC-TT with a thieno[3,2-b]thiophene moiety, and BTTIC-Ph with a benzene moiety.[137] Due to the larger dihedral angle between benzene (or thieno[3,2-b]thiophene) and the ladder-type fused-ring skeleton, BTTIC-Ph and BTTIC-TT displayed an upshifted LUMO value relative to BTTIC-Th. The PM6:BTTIC-Ph blend presented different types of π–π stacking and larger domain size, which are detrimental for carrier transport and exciton dissociation. Finally, the BTTIC-TT-based device achieved the best device efficiency of 13.44% and the BTTIC-Th-based device achieved a high efficiency of 12.91%, which is obviously superior to that of the BTTIC-Ph-based device (9.14%). In addition, they compared the impact of thiophene chains and alkoxyl side chains on acceptors' properties and device performance, and found that BTOIC with alkoxyl chains shows redshifted absorption and elevated energy levels relative to those of BTTIC, which could be ascribed to the strong electron donating ability of alkoxyl chains.[138] Furthermore, BTOIC showed intense crystallinity, resulting in a rough surface morphology and oversize domain size, leading to a low PCE of 10.96%.

The asymmetric side-chain strategy is a useful way to improve cell efficiency. For instance, A. K.-Y. Jen and co-workers developed three SMAs with asymmetric side chains, namely, TOBDT with a thiophene side chain and an alkoxyl side chain, POBDT-4Cl with a phenylalkyl chain and an octyloxy chain, and COBDT-4Cl with a phenylalkyl chain and a flexible octyl chain.[139,140] COBDT-4Cl showed slightly redshifted absorption and elevated energy levels, enhanced molecular packing and electron mobility compared to TOBDT and POBDT-4Cl. The PM6:COBDT-4Cl device achieved the highest efficiency of 13.5% and an E_{loss} of 0.52 eV.

In addition to introducing heteroatoms such as fluorine, chlorine, sulfur, etc. into the side chain, silicon atoms were also introduced into the thiophene side chain of BDT-based SMAs to tune the materials' properties. Zhan's group developed two BDT-based SMAs of IN-4F tri(n-propyl)silylthienyl side chains and ISI-4F with tri(n-propyl)silylethynyl side chains.[141] Owing to the significant contribution of the ethynyl group in HOMO and LUMO orbitals, ISI-4F presented blue-shifted absorption spectra and upshifted molecular energy levels as compared with IN-4F. The OSCs based on PM6:ISI-4F delivered PCEs of 12.5%, slightly lower than that of IN-4F-based device (13.0%) due to the reduced FF.

Swapping the position of alkyl side chains has a great impact on the acceptors' physicochemical properties. Hou et al. added another alkyl chain to 2D thiophene side chains at different positions to modulate the steric hindrance and electron accepting and donating properties.[142] In BTCN-O, the alkyl chain is attached to the 4-position, whereas in BTCN-M, the alkyl chain
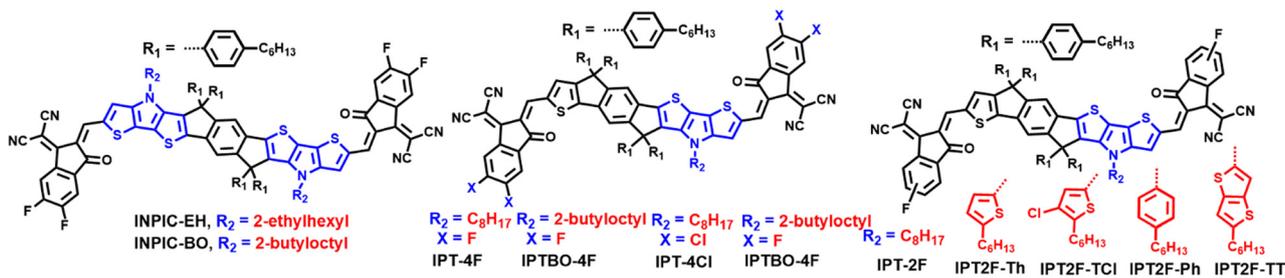
is introduced at the 3-position. With this subtle change, the dihedral angle between the 2D thiophene chain in BTCN-O and the BDT unit is smaller than that of BTCN-M (59° versus 70°). BTCN-O presents much redshifted absorption in films and an elevated HOMO value, and enhanced hole mobility but much lower electron mobility compared to BTCN-M. Thus, the PBDB-T:BTCN-M blend achieved a better efficiency of 5.89% compared to the PBDB-T:BTCN-O blend (1.62%), where BTCN-M shows electron accepting properties, and the BTCN-O:PC$_{71}$BM blend yielded a better efficiency of 6.68% compared to BTCN-M:PC$_{71}$BM (0.29%), where BTCN-O shows electron donating properties.

Side-chain engineering on M-series acceptors is of significant importance for boosting device performance, where the central core of M-series acceptors typically consists a BDT unit and two N alkyl chains.[156–158] In this part, Zheng and co-worker did some nice work. First, they fixed the alkyl chain on the nitrogen as 2-ethylhexyl and changed the length of alkoxyl on the BDT unit to obtain two SMAs of M2 with 2-ethylhexyloxy and M4 with 2-butyloctyloxy.[143] Despite the different side chain on BDT, two SMAs showed similar optical bandgaps and energy levels. However, the device based on PM6:M4 realized better PCE (14.75%) than the M2-based device (11.16%) because of the more balanced charge transport. Next, based on M2, they developed two new SMAs (M36 and M38) by simultaneously increasing the length of alkyl-chains on N and O, and ensuring that both alkyl chains were of the same length.[144] M38 with 2-decyltetradecyl chains showed obviously blue-shifted absorption in films and broader bandgaps compared to M2 with 2-ethylhexyl chains and M36 with 2-butyloctyl chains. Compared to M2 and M38 with too short or too long side chains, M36 presented the most ordered and closest π–π stacking, which is favorable to charge transport; thus the PM6:M36 device achieved the highest PCE of 16.00%. Finally, they fixed the alkyl chain on BDT as 2-ethylhexyl and changed the alkyl chains on N to acquire two SMAs, namely, M3 and M32.[145] The relation and difference between M3 and M32 in chemical structures is that these two SMAs are a pair of isomers, the alkyl chain on N of M3 is a branched chain, while for M32, it is a linear chain. Compared with M32 (edge-on molecular orientation), M3 exhibits a significantly different molecular orientation (face-on) and enhanced electron mobility. Consequently, the PM6:M3 device yielded a record efficiency of 16.6% for the A–D–A type SMA-based device.

2.4. Side-chain engineering of DTP-based SMAs

Due to the electron-donating properties of nitrogen atoms, dithieno[3,2-b:2′,3′-d]pyrrol (DTP) has widely been used as a building block to develop narrow bandgap nonfullerene SMAs with higher LUMO energy levels.[146–149] In 2018, Tang and co-workers reported a DTP-based nonacyclic SMA of INPIC-4F with two linear C8 side chains which achieved a high PCE of 13.1%.[146] Later, they replaced the linear chains with branched alkyl side chains (2-ethylhexyl (EH) and 2-butyloctyl (BO)) to obtain two new SMAs of INPIC-EH and INPIC-BO (Fig. 10).[147] Altering the side chains in INPIC had little effect on electrochemical and optical properties. However, the INPIC-EH- and

2742 | Energy Environ. Sci., 2023, **16**, 2732–2758

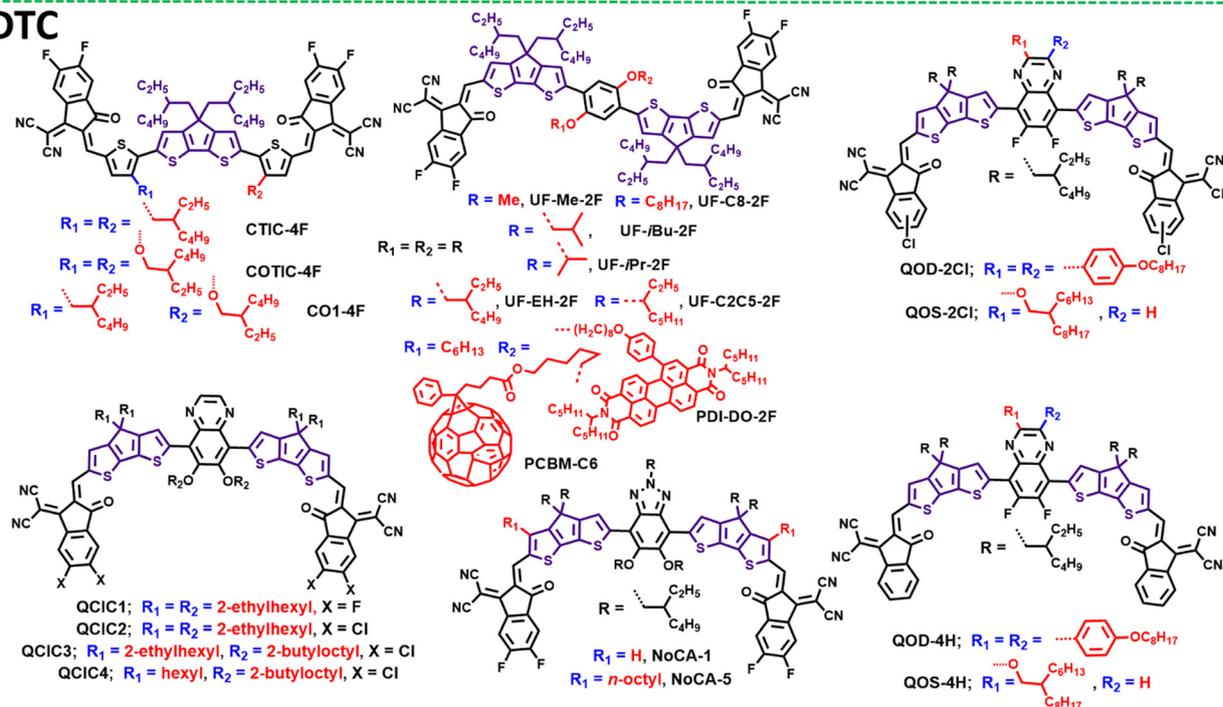This journal is © The Royal Society of Chemistry 2023

Fig. 10 Chemical structures of DTP- and DTC-based SMAs with different side chains.

INPIC-BO-based OSCs gave obviously lower PCE (PCE = 11.9% for INPIC-EH; PCE = 11.2% for INPIC-BO) than that of INPIC-based device (Table 5), originating from the oversize phase separation in PBDB-T:INPIC-BO and PBDB-T:INPIC-EH blends.

In 2019, Tang *et al.* reported an asymmetric heptacyclic core by removing the peripheral thieno[3,2-*b*]pyrrole unit of the central core in INPIC, and employed the new core to obtain a SMA of IPT-2F with an efficiency of 14%.[148] Based on IPT-2F containing DTP, the same team developed four asymmetric SMAs (IPTBO-4F, IPT-4F, IPTBO-4Cl, and IPT-4Cl) through fine regulation of the terminal accepting units and side chains.[149] As a result, IPT-4F- and IPTBO-4Cl-based devices delivered a higher and similar PCE of 15% due to the balanced molecular packing and aggregation, as compared with IPTBO-4F and IPT-4Cl. Replacing an alkyl chain with an aryl side chain is a common approach to tune the device efficiency. Then, they first incorporated 2D conjugated chains into the asymmetric IPT central core by replacing linear *n*-octyl in IPT-2F with 3-chloro-2-hexylthienyl to acquire a new SMA of IPT2F-TCl.[150] The OSCs based on PBDB-T:IPT2F-TCl realized a decent PCE and an outstanding FF of

77.51%. The high FF can be mainly ascribed to the large electron (μ_e) and hole (μ_h) mobility, and nearly symmetric charge transport (μ_e/μ_h = 1.02) in the PBDB-T:IPT2F-TCl blend. Apart from using 3-chloro-2-hexylthienyl as side chains, they systematically compared the three asymmetric acceptors (IPT2F-TT, IPT2F-Ph and IPT2F-Th) with different N-conjugated side chains (4-hexylphenyl, 5-hexylthiophen-2-yl, and 5-hexylthieno[3,2-*b*]thiophen-2-yl).[151] These three SMAs showed similar optical and electrochemical properties. After blending these SMAs with PBDB-T separately, IPT2F-TT containing TT side chains yielded the highest PCE of 14.02%, performing better than the devices based on phenylated IPT2F-Ph (13.11%) and thineylated IPT2F-Th (12.52%). The best PCE of the IPT2F-TT-based device should be attributed to the better morphology, including the dominated face-on orientation, proper phase separation with interpenetrating network structures.

2.5.   Side-chain engineering of DTC-based SMAs

Employing dithieno[3,2-*b*:2′,3′-*d*]cyclopentadiene to exploit unfused SMAs has attracted significant attention. For example, Bo and co-workers developed a series of non-fused SMAs based

Table 5 Optical, electrochemical and photovoltaic data of DTP- and DTC-based nonfullerene SMAs with different side chains

SMA	$E_g^{\text{opt}\,a}$ (eV)	HOMO[b]/LUMO[b] (eV)	Donor	V_{OC} (V)	J_{SC} (mA cm^{-2})	FF	PCE%	Ref.
INPIC-4F	1.39	−5.42/−3.95	PBDB-T	0.852	21.9	0.694	13.1	146
INPIC-EH	773	−5.48/−3.99	PBDB-T	0.837	20.7	0.684	11.9	147
INPIC-BO	776	−5.47/−3.97	PBDB-T	0.839	20.0	0.668	11.2	147
IPT-4F	1.42	−5.57/−4.08	PM6	0.914	22.08	0.7415	14.96	148
IPTBO-4F	1.41	−5.57/−4.07	PM6	0.917	22.08	0.7245	14.67	149
IPT-4Cl	1.39	−5.58/−4.11	PM6	0.883	23.18	0.7037	14.40	149
IPTBO-4Cl	1.39	−5.64/−4.08	PM6	0.893	23.15	0.7257	15.00	149
IPT2F-ThCl	1.48	−5.59/−4.00	PBDB-T	0.86	20.59	0.7751	13.74	150
IPT2F-Th	1.47	−5.58/−4.03	PBDB-T	0.86	20.44	0.7120	12.52	151
IPT2F-Ph	1.46	−5.57/−4.00	PBDB-T	0.86	21.18	0.7211	13.13	151
IPT2F-TT	1.45	−5.60/−4.00	PBDB-T	0.84	22.24	0.7506	14.02	151
DOC6-IC	1.43	−5.33/−3.72	PBDB-T	0.91	19.21	0.6011	10.52	152
DOC8-IC	1.39	−5.36/−3.71	PBDB-T	0.92	17.74	0.5765	9.41	152
DOC2C6-IC	1.44	−5.38/−3.73	PBDB-T	0.93	18.85	0.6333	11.10	152
DC6-IC	1.69	−5.53/−3.79	PBDB-T	0.99	11.19	0.6221	6.87	152
UF-EH-2F	1.38	−5.49/−4.11	J52	0.79	24.87	0.69	13.56	153
QOD-4H	1.45	−5.61/−3.77	PBDB-T	0.843	17.04	0.4834	6.94	154
QOD-2Cl	1.43	−5.61/−3.81	PBDB-T	0.824	20.74	0.6244	10.67	154
QOS-4H	1.43	−5.55/−3.70	PBDB-T	0.893	16.74	0.5355	8.01	154
QOS-2Cl	1.43	−5.60/−3.77	PBDB-T	0.845	21.03	0.6870	12.19	154
QCIC1	1.41	−5.52/−3.80	PBDB-T	0.822	18.81	0.555	8.58	155
QCIC2	1.39	−5.53/−3.84	PBDB-T	0.807	18.65	0.603	9.09	155
QCIC3	1.38	−5.52/−3.89	PBDB-T	0.816	19.39	0.669	10.55	155
QCIC4	1.35	−5.49/−3.90	PBDB-T	0.780	19.16	0.638	9.53	155
CTIC-4F	1.3	−5.4/−4.0	PTB7-Th	0.70	23.4	0.64	10.5	156
CO1-4F	1.2	−5.3/−4.1	PTB7-Th	0.64	24.8	0.64	10.0	156
COTIC-4F	1.1	−5.2/−4.1	PTB7-Th	0.57	20.7	0.61	7.3	156
NoCA-1	—	−5.34/−3.43	J52	0.769	24.69	0.6169	11.71	157
NoCA-5	—	−5.30/−3.38	J52	0.814	26.02	0.6996	14.82	157
PDI-DO-2F	1.44	−5.54/−3.69	PBDB-T	0.89	20.04	0.6618	11.78	158
PCBM-C6	1.43	−5.26/−3.84	PBDB-T	0.86	20.41	0.7115	12.51	159
PCBM-C10	1.41	−5.27/−3.84	PBDB-T	0.87	21.30	0.7206	13.55	159

[a] Calculated from $E_g^{\text{opt}} = 1240/\lambda_{\text{onset}}$. [b] Calculated from CV curves.

on a central 2,5-bis(alkyloxy)phenylene core, two DTC spacerrs, and two terminal accepting groups.[152] Due to the multiple S···O non-covalent interactions, DOC6-IC, DOC8-IC and DOC2C6-IC showed markedly larger fluorescence quantum yields and lower band gaps relative to those of DC6-IC (Fig. 10). The OSCs based on PBDB-T:DOC2C6-IC exhibited a better PCE of 11.10%, higher than that of the device based on PBDB-T:DOC6-IC (10.52%) and PBDB-T:DOC8-IC (9.41%). Notably, these three devices gave small non-radiative recombination losses of ~0.21 eV, obviously lower than those of the DC6-IC-based device (0.30 eV). After fluorination of DOC2C6-IC, the generated DOC2C6-2F exhibited an enhanced PCE of 13.24%. Similar work was reported by Chen and co-workers, and they also confirmed that the SMA (UF-EH-2F) with 2-ethylhexyl side chains exhibited better device performance.[153]

Yang and co-workers synthesized four unfused SMAs (QOD-4H, QOS-4H, QOD-2Cl, and QOS-2Cl) based on DTC and quinoxaline with different terminal units and side chains.[154] In particular, the branched alkyl chains in two QOS-based acceptors exhibited reduced crystallization tendency but smaller π–π stacking distances relative to those of the two QOD-based SMAs. This trend was also observed through the chlorination of QOD(s)-4H. When these four SMAs were paired with PBDB-T, the QOS-2Cl-based device achieved the highest PCE of 12.19%, resulting from the tightest molecular packing and the clearest nanofibrillar networks. Chen et al. also reported four unfused SMAs

(QCIC1, QCIC2, QCIC3, and QCIC4) with the same backbone as the abovementioned QOD-4H, but different alkyl chains.[155] Thanks to the more and the longer branched chains, the blend of PBDB-T and QCIC3 demonstrated the best molecular packing and an optimal domain size, which endowed the PBDB-T:QCIC3 device to with the best PCE of 10.55%, when compared to the other three group devices.

Unlike other non-fused SMAs with DTC as a π-spacer, Bazan and co-workers developed a non-fused SMA of COTIC-4F with DTC as the central core, and they studied the impact of side chains on physicochemical properties and device parameters of SMAs based on the COTIC-4F backbone.[156] By progressively replacing the alkoxy side chain in COTIC-4F with alkyl groups, two new SMAs, CO1-4F and CTIC-4F, were obtained. Because of the electron-donating characteristic of alkoxy side chains, the optical band gaps gradually increased from COTIC-4F, CO1-4F, to CTIC-4F. The OSCs based on PTB7-Th: CTIC-4F and PTB7-Th:CO1-4F delivered PCEs of over 10% along with impressive J_{SC}s of 25 mA cm^{-2}, outperforming than the COTIC-4F-based devices.

Incorporation of an alkyl chain into the outermost aromatic ring of the central core in IDTT-based SMAs to restrict the rotation of the terminal units is an important means to boost the device efficiency. This strategy has also been proven effective in DTC-based non-fused SMAs. Huang and co-workers introduced an n-octyl group at the ß position of thiophene in

DTC, and developed a new SMA of NoCA-5.[157] Compared with unoctylated NoCA-1, NoCA-5 demonstrated an upshifted LUMO value, enhanced crystallinity and smaller reorganization energy due to better molecular rigidity. Finally, the devices based on NoCA-5 achieved a high efficiency of 14.82%, significantly better than that of the NoCA-1-based one (11.71%).

It is feasible to develop high-performance non-fused ring electron acceptors by using large aromatic rings as side chains.[158,159] For example, Bo and co-workers reported a non-fused ring SMA of PDI-DO-2F by attaching perylenediimide (PDI) units as a side chain. Compared to DO-2F with alkyl side chains on the central benzene ring, PDI-DO-2F showed improved solubility, enhanced fluorescence quantum yield and decreased crystallinity, endowing PDI-DO-2F with better PCE and lower nonradiative energy loss.[158] Furthermore, they developed two non-fused ring SMAs with PCBM as the side group, namely, PCBM-C6 and PCBM-C10.[159] The addition of bulky and electronically isotropic fullerene side groups to the SMAs was found to be an effective strategy to suppress severe aggregation behaviors and improve the active-layer morphology. This approach resulted in enhanced efficiencies for charge collection and exciton separation compared to the control molecule of CH3COO-C6. Consequently, the use of fullerene pendants resulted in simultaneous improvements in the V_{OC}, J_{SC}, and FF values of the solar cells. These enhancements led to a significantly increased PCE of 13.55% in the PCBM-C10-based device.

2.6. Side-chain engineering of oligothiophene-based non-fused SMAs

Oligothiophenes have become the mainstream backbones for the construction of non-fused SMAs.[160–164] Bo and co-workers developed four tetrathiophene-based non-fused ring SMAs, namely 4T-1, 4T-2, 4T-3, and 4T-4, with different lengths of the lateral side chains (Fig. 11).[160] In a dilute chlorobenzene (CB) solution, the four acceptors showed similar absorption

curves. In the solid state, 4T-1 exhibited remarkably redshifted absorption spectra due to the strong molecular packing, as compared with the ones in solution, while for the other three SMAs, because of the steric hindrance of the 2-ethylhexyl chains, the red shift of the absorption spectra of the acceptors was not obvious and the intermolecular packing was not as tight as 4T-1. As a result, the PBDB-T:4T-3 device delivered a decent PCE of 10.15% (Table 6), resulting from the better compatibility between PBDB-T and 4T-3. During the same period, the same group reported two SMAs (o-4TBC-2F and m-4TBC-2F) built on tetrathiophene backbones, by altering the hexyloxy side-chain position in phenyl groups.[161] o-4TBC-2F containing ortho-hexyloxy-phenyl chains displayed a more planar molecular structure, narrower band gap, and better molecular packing and orientation relative than m-4TBC-2F with meta-hexyloxy-phenyl chains. The PBDB-T:o-4TBC-2F cell yielded a good efficiency of 10.26%, performing better than the device based on m-4TBC-2F (2.63%).

Hou et al. also synthesized and reported three tetrathiophene-based non-fused ring SMAs (A4T-16, A4T-21, A4T-23) with different phenyl substituted side chains, including 2,4,6-triisopropylphenyl (Pi), 2,4,6-trimethylphenyl, and unsubstituted benzene.[162] Pi endowed A4T-16 with good molecular planarity and large steric hindrance, leading to the three-dimensional charge transport, as confirmed by the single-crystal data of A4T-16. When the three SMAs were paired with PM6, the device based on A4T-16 realized a high efficiency of 15.2%, representing the best value for the fully non-fused SMA-based OSCs.

Apart from employing tetrathiophene as a backbone to develop non-fused ring SMAs, thieno[3,2-b]thiophene (TT) is also a commonly used building block to construct non-fused ring acceptors. For instance, Bo and co-workers first employed diphenylamine derivatives as side chains to prepare four non-fused SMAs, namely, H-2F, CH$_3$-2F, OCH$_3$-2F, and SCH$_3$-2F.[163]
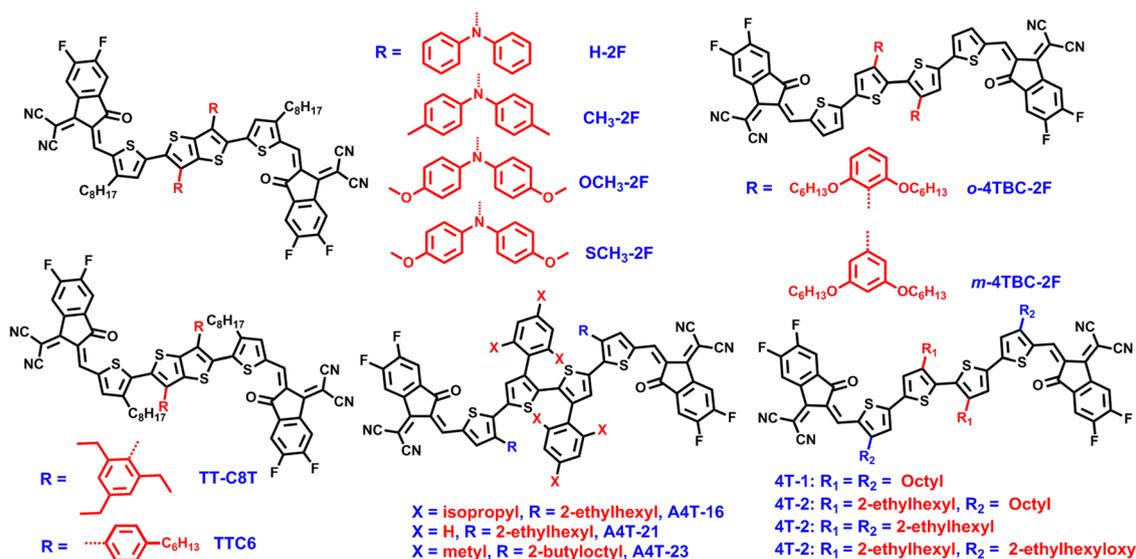

Fig. 11 The chemical structures of oligothiophene-based non-fused SMAs with different side chains.

This journal is © The Royal Society of Chemistry 2023

Energy Environ. Sci., 2023, **16**, 2732–2758 | **2745**

Table 6 Optical, electrochemical and photovoltaic data of oligothiophene-based SMAs with different side chains

SMA	$E_g^{\text{opt }a}$ (eV)	HOMO^b/LUMO^b (eV)	Donor	V_{OC} (V)	J_{SC} (mA cm^{-2})	FF	PCE%	Ref.
4T-1	1.47	−5.71/−4.09	PBDB-T	0.84	12.70	0.5171	5.53	160
4T-2	1.54	−5.85/−4.02	PBDB-T	0.82	15.68	0.7032	9.09	160
4T-3	1.52	−5.86/−3.98	PBDB-T	0.81	17.27	0.7245	10.15	160
4T-4	1.60	−5.85/−3.86	PBDB-T	0.94	14.27	0.6182	8.27	160
o-4TBC-2F	1.47	−5.63/−4.00	PBDB-T	0.76	20.48	0.657	10.26	161
m-4TBC-2F	1.66	−5.68/−4.00	PBDB-T	0.84	7.90	0.400	2.63	161
A4T-16	1.45	−5.67/−3.96	PM6	0.876	21.8	0.798	15.2	162
A4T-21	1.66	−5.89/−3.92	PM6	0.936	5.55	0.303	1.57	162
A4T-23	1.43	−5.63/−3.98	PM6	0.870	21.0	0.568	10.4	162
H-2F	1.46	−5.58/−4.06	PBDB-T	0.73	18.78	0.6299	8.64	163
CH$_3$-2F	1.42	−5.59/−4.01	PBDB-T	0.77	22.76	0.6985	12.28	163
OCH$_3$-2F	1.33	−5.40/−4.04	PBDB-T	0.74	16.66	0.6463	8.01	163
SCH$_3$-2F	1.41	−5.50/−4.06	PBDB-T	0.67	15.38	0.6494	6.67	163
TTC6	1.73	−5.79/−3.93	D18	0.93	10.20	0.463	4.41	164
TT-C8T	1.55	−5.77/−3.91	D18	0.91	19.31	0.591	10.42	164
TT-TC8	1.44	−5.79/−3.90	D18	0.86	23.06	0.662	13.13	164

^{a} Calculated from $E_g^{\text{opt}} = 1240/\lambda_{\text{onset}}$. ^{b} Calculated from CV curves.

The incorporation of diphenylamine improved the molecular solubility, prevented the formation of oversized self-aggregates, and boosted the ICT effect. Different substituents (H, –CH$_3$, –SCH$_3$, and –OCH$_3$) on diphenylamine of the four acceptors have great impact on physicochemical properties and cell efficiency (Fig. 12). Compared with the other three SMAs, methylated CH$_3$-2F showed stronger absorption ability in a solid state, better molecular orientation and π–π stacking.

Due to the strongest electron-donating ability of methoxy, OCH$_3$-2F exhibited the lowest bandgap and shallowest HOMO energy level. A two-dimensional change transport mode was observed in CH$_3$-2F and validated by the single-crystal data, which resulted from intermolecular non-covalent interactions of S···π, N···N, F···F and π···π. It is because of these advantages that the device based on PBDB-T:CH$_3$-2F achieved the highest efficiency of 12.28%, higher than those of the
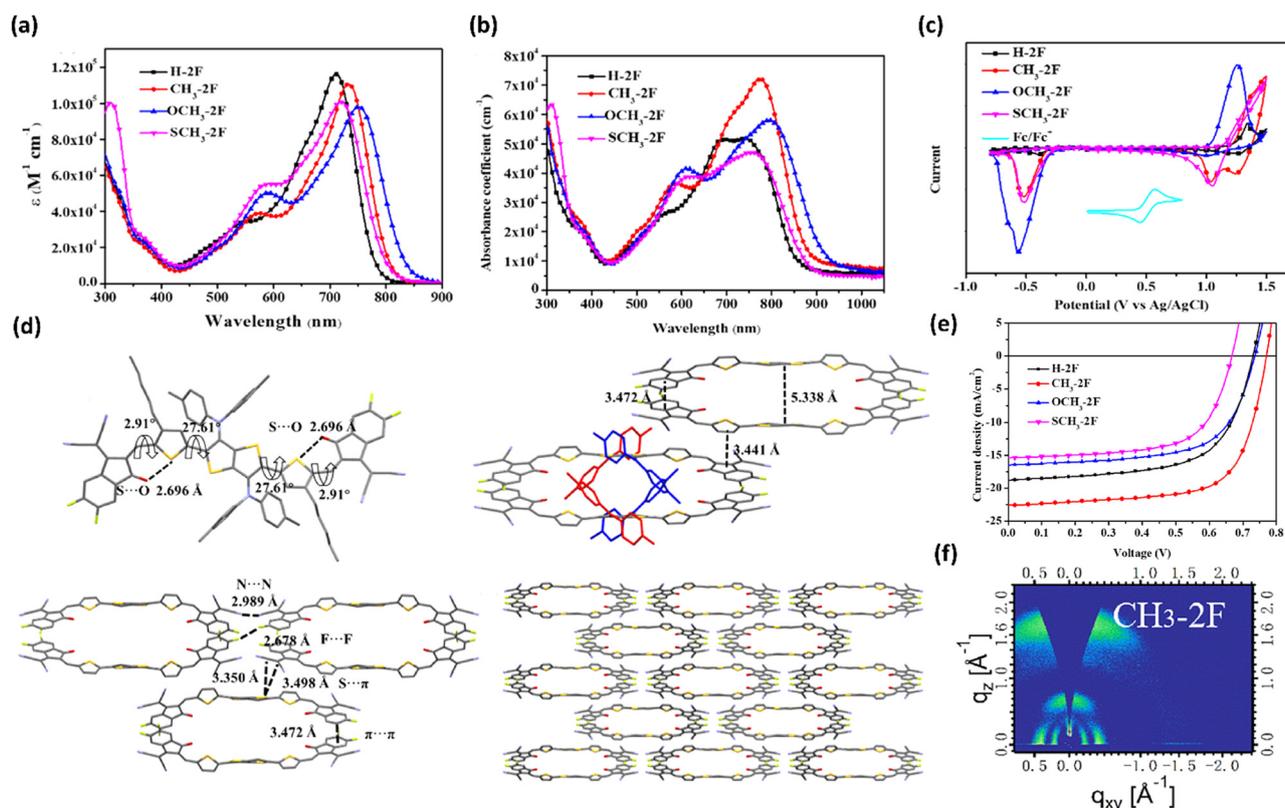
Fig. 12 (a) Absorption spectra of H-2F, CH$_3$-2F, OCH$_3$-2F, and SCH$_3$-2F in solutions; (b) Absorption spectra and CV curves (c) of H-2F, CH$_3$-2F, OCH$_3$-2F, and SCH$_3$-2F in films; (d) Single-crystal structure of CH3-2F; (e) J–V curves of H-2F-, CH$_3$-2F-, OCH$_3$-2F-, and SCH$_3$-2F-based devices; (f) 2D GIWAXS patterns of the neat CH$_3$-2F acceptor. Adapted with permission.[163] Copyright 2021, American Chemical Society.

2746 | *Energy Environ. Sci.*, 2023, **16**, 2732–2758

This journal is © The Royal Society of Chemistry 2023

Fig. 13 The chemical structures of Y6 and BTP.

H-2F-based device (8.64%), OCH$_3$-2F-based device (8.01%), and SCH$_3$-2F-based device (6.67%). The high PCE of the CH$_3$-2F-based device is mainly ascribed to the significant face-to-face molecular orientation, suitable phase separation and low energy loss. Additionally, they compared the effects of 4-hexyl-phenyl and 2,4,6-triethylphenyl on the TT of two SMAs (TTC6 and TT-C8T) on the device performance, and found that 2,4,6-triethylphenyl endowed TT-C8T with good molecular planarity, higher electron mobility, more favorable molecular orientation, and better device performance.[164]

3. Side-chain engineering of A–DA$_1$D–A-type nonfullerene SMAs

In comparison with traditional A–D–A structured SMAs, A–DA$_1$D–A type SMAs usually demonstrate lower band gaps and smaller energy loss due to intramolecular multiple D–A interactions and high fluorescence quantum yields. The most common A–DA$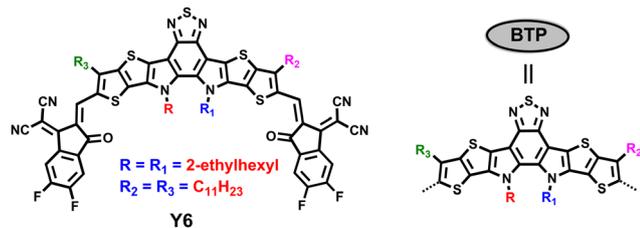_1$D–A type SMAs include benzo[c][1,2,5]thiadi-azole (BT)-, benzotriazole (BTZ)- and quinoxaline(Qx)-based ones. In this part, we mainly introduce side-chain engineering of BT- and BTZ-based SMAs.

3.1. Side-chain engineering of BT-based SMAs

Y6,[10] as a typical BT-based SMA, has four relatively independent alkyl chains: two of them are distributed at the β position of the outer thiophene, and the other two are located on the nitrogen atom of the pyrrole ring (Fig. 13). Modifying the side chains on the nitrogen atom or at the β position of the outer thiophene in A–DA$_1$D–A type SMAs is a simple and useful way to boost device efficiency.

At the N position, Zou et al. altered the N alkyl chains to linear chains and different branching position chains. N-C11 with linear chains exhibited much inferior solubility and excessive aggregation.[165] N4 (Fig. 14) with 4th-position branched chains showed larger domain size and predominantly edge-on orientation when blended with PM6. N3 with 3rd-position branched chains delivered an optimum morphology, and the binary device based on N3 achieved a PCE of 15.98% (Table 7), and the PM6:N3:PC$_{71}$BM ternary device achieved a PCE of 16.74%. Altering the branching point of N alkyl chains in Y6 was also reported by our group, and similar results were obtained, that is, the devices based on Y6-C2 (or N3) realized the highest PCEs as compared with Y6 and Y6-C3 (or N4).[166]

Apart from branching position, regulating the length of branched side chains is also a main direction for optimizing the molecular structure. For example, Yao et al. finely modified the inner branched side chain length of chlorinated SMAs for superior processability. The 2-butyloctyl chains in BTP-4Cl-12 could balance the solution processability and aggregation behavior.[167] The PBDB-TF:BTP-4Cl-12 device achieved a PCE of 17.0% via spin-coating process and 15.5% via blade-coating process in a 1 cm^2 device. Similarly, He et al. synthesized four chlorinated SMAs with different alkyl chain lengths on the inner side chains. BTIC-HD-4Cl and BTIC-BO-4Cl exhibited good solubility in comparison to BTIC-C12-4Cl with linear alkyl chains and branched short alkyl-substituted BTIC-EH-4Cl.[168] BTIC-BO-4Cl showed relatively red-shifted absorption spectra and enhanced absorption capacity and short (010) stacking distance in the PM6:acceptor blend. The cell based on BTIC-BO-4Cl presented the best PCE of 16.43%. In addition, Gao et al. tuned the branched alkyl chain length in the inner N alkyl chains with naphthalene-fused end groups.[169] Compared with BTP-C4C6-N with 2-butyloctyl and BTP-C6C8-N with 2-hexyl-decyl, BTP-C2C4-N with 2-ethylhexyl chains presented red-shifted absorption in films and the strongest crystallinity. The PM6:BTP-C4C6-N device delivered an efficiency of 12.4%, higher than those of BTP-C6C8-N- and BTP-C2C4-N-based devices (10.3% and 11.9%, respectively). Besides, the three SMAs with naphthalene-fused end groups can help reduce the nonradiative recombination energy loss.

Introducing highly polarizable OEG groups into SMAs can increase the solubility of the resulting molecules in non-halogenated solvents. Li et al. replaced the inner alkyl side chains of Y6 with amphiphilic OEG chains to get BTO.[170] BTO exhibited better solubility in non-halogenated paraxylene, higher coplanarity, and a more ordered film induced by OEG chains. BTO showed excellent compatibility with the Y6 host, and Y6 : BTO (1 : 0.2) exhibited reinforced crystallinity. By using this guest-assisted assembly strategy, PM6:Y6:BTO achieved a high PCE of over 16% in chlorobenzene (CB) and PX solvent, and the PCE of the PM6:Y6:BTO:PC$_{71}$BM device was further increased to over 17%. Impressively, the PM6:Y6:BTO:PC$_{71}$BM large-area module (36 cm^2) showed a record PCE of 14.26% for OSCs with the module area > 20 cm^2.

Above, we discussed the case where the two alkyl chains on the nitrogen of BT-based SMAs are the same; when the two alkyl chains on the nitrogen are different, then a molecule with asymmetric alkyl chains is formed. Taking Y6-4O as an example, Lin et al. tailored the inner alkyl side chains of Y6 to asymmetric highly polarizable OEG and alkyl side chains to get Y6-4O.[171] Compared with Y6, Y6-4O showed a larger dipole moment, higher dielectric constant, excellent solubility in halogen-free solvents, and tendency toward face-on orientation. The toluene-processed PM6:Y6-4O as-cast device delivered lower energy loss, a higher exciton dissociation rate, and a smaller bimolecular recombination ratio, resulting in an improved device efficiency of 15.2%.

Huang et al. adopted a strategy to utilize asymmetric inner side chains to boost the photovoltaic performance.[172] Compared to BO-4F with symmetric 2-butylocyl chains, Bu-OD-4F with
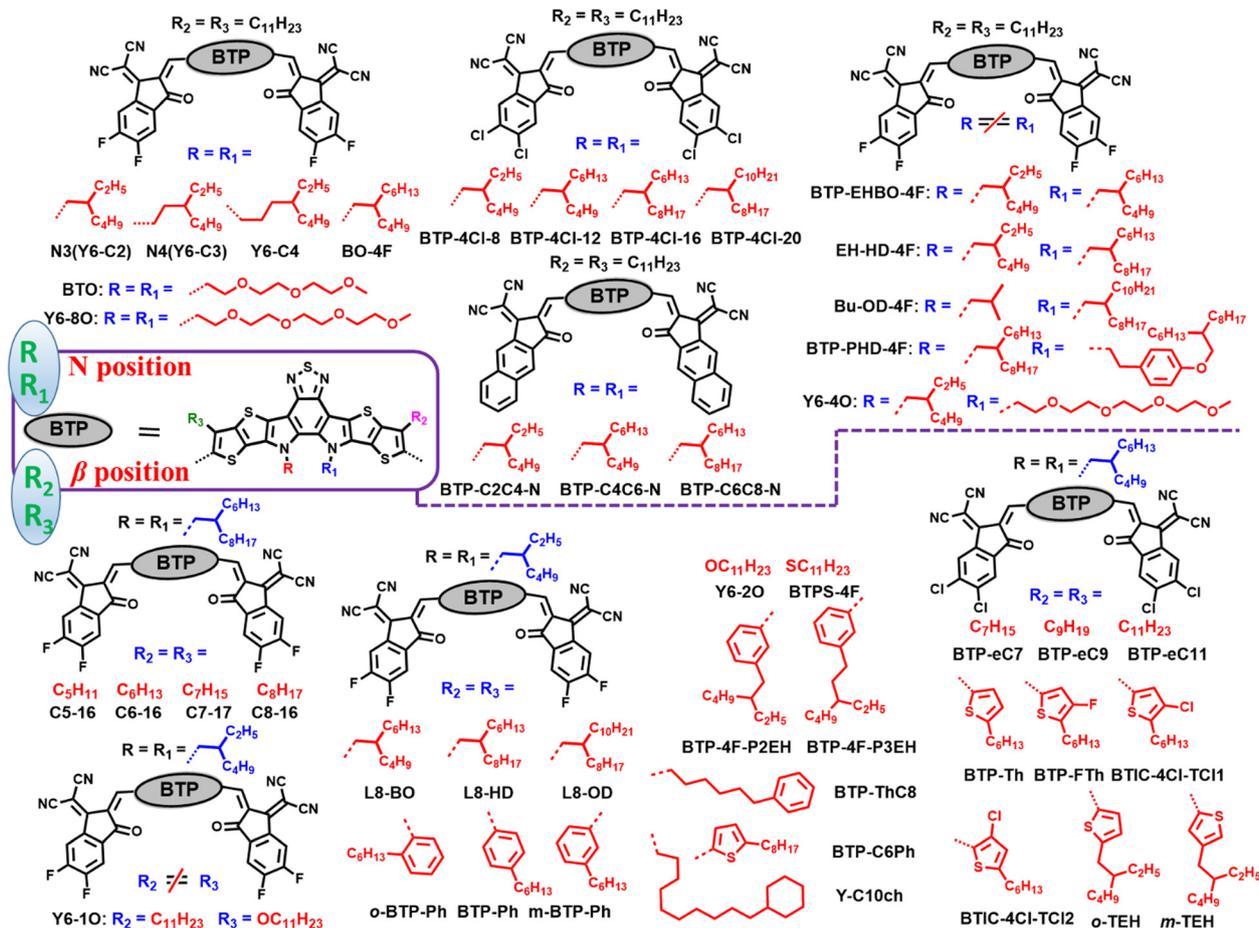
This journal is © The Royal Society of Chemistry 2023

Energy Environ. Sci., 2023, 16, 2732–2758 | 2747

Fig. 14 Chemical structures of BT-based SMAs with different side chains.

Table 7 Optical, electrochemical and photovoltaic data of BT-based A−DA$_1$D−A SMAs with different side chains at the N position

SMA	$E_g^{\text{opt } a}$ (eV)	HOMO^b/LUMO^b (eV)	Donor	V_{OC} (V)	J_{SC} (mA cm^{-2})	FF	PCE%	Ref.
N3	—	—	PM6	0.837	25.81	0.739	15.98	166
Y6	1.33	−5.67/−4.08	PM6	0.859	25.22	0.703	15.24	166
Y6-C2	1.33	−5.65/−4.09	PM6	0.860	25.11	0.736	15.98	167
Y6-C3	1.41	−5.68/−4.07	PM6	0.852	24.07	0.674	13.76	167
BTP-4Cl-8	—	−5.67/−4.11	PBDB-TF	0.872	25.2	0.743	16.3	168
BTP-4Cl-12	—	−5.66/−4.09	PBDB-TF	0.858	25.6	0.776	17.0	168
BTP-4Cl-16	—	−5.68/−4.09	PBDB-TF	0.862	24.2	0.748	15.6	168
BTIC-BO-4Cl	1.34	−5.54/−4.14	PBDB-TF	0.85	25.26	0.7625	16.43	169
BTP-C2C4-N	1.34	−5.49/−3.90	PM6	0.93	18.2	0.571	10.3	170
BTP-C4C6-N	1.35	−5.50/−3.90	PM6	0.94	20.7	0.621	12.1	170
BTP-C6C8-N	1.35	−5.50/−3.88	PM6	0.95	20.2	0.620	11.9	170
EH-HD-4F	1.39	−5.69/−4.04	PM6	0.84	27.5	0.793	18.38	172
BO-4F	1.40	−5.70/−4.01	PM6	0.84	27.0	0.767	17.39	172
Bu-OD-4F	1.42	−5.68/−4.01	PM6	0.85	26.2	0.766	17.10	172
BTP-EHBO-4F	1.33	−5.80/−3.97	PM6	0.85	26.12	0.7578	16.82	173
BTP-PHD-4F	1.30	−5.79/−3.95	PM6	0.87	25.64	0.7134	15.91	173

^{a} Calculated from $E_g^{\text{opt}} = 1240/\lambda_{\text{onset}}$. ^{b} Calculated from CV curves.

asymmetric 2-octyldodecyl and 2-butyl chains showed relatively blue-shifted absorption and poor miscibility in blends, an EH-HD-4F with asymmetric 2-hexyldecyl and 2-ethylhexyl chains showed slightly red-shifted absorption and favorable morphology in blends. The device based on EH-HD-4F achieved the best efficiency of 18.38%, which is better than that of the device based on Bu-OD-4F (17.10%) and BO-4F (17.39%). In addition, Hsu *et al.* adopted a strategy utilizing asymmetric inner *N* alkyl chains, namely, 2-ethylhexyl and 2-butyloctyl chains for BTP-EHBO-4F and 2-hexyldecyl and phenyl alkoxy chains for

2748 | *Energy Environ. Sci.*, 2023, **16**, 2732–2758

This journal is © The Royal Society of Chemistry 2023

BTP-PHD-4F.[173] In comparison with Y6, BTP-PHD-4F and BTP-EHBO-4F showed an obviously enhanced absorption coefficient and stronger molecular π–π interactions. PM6:BTP-PHD-4F and PM6:BTP-EHBO-4F devices achieved much higher PCEs of 15.91% and 16.82% compared to the PM6:Y6 device with o-xylene as green solvent.

Focusing on the β-position side chains of the outer thiophene in BT-based A–DA$_1$D–A acceptors, many high-efficiency SMAs have emerged by modifying the outer side chains. Yao et al. investigated the impact of the outer linear side-chain length on photovoltaic performance. By gradually tailoring the alkyl chains from C11 to C9, then to C7, BTP-eC9 maintained good solubility and enhanced intermolecular ordering. BTP-eC7 exhibited lower solubility, more ordered packing, and excessive aggregation in blends.[85] The device based on BTP-eC9 achieved the highest efficiency of 17.8% because of the simultaneously increased J_{SC} and FF (Table 8). Wang et al. developed four nonfullerene acceptors (C5–16, C6–16, C7–16, and C8–16) by meticulously tailoring the outer thiophene alkyl chains (from C5–C8), investigated their aggregation and optoelectronic properties.[174] With the decrease in the alkyl-chain length, the molecular energy levels were gradually downshifted and the absorption spectra almost remained unchanged. BTP-4F-C5–16 presented the strongest intermolecular π–π stacking and

highest electron mobility, leading to the highest efficiency of 18.20% in the PM6:BTP-4F-C5–16 device.

Sun et al. replaced the outer linear side chains of Y6 with bulk branched side chains, and investigated the branched side-chain length effect on molecular packing.[72] Compared with Y6, L8-BO (2-butyloctyl substitution), L8-HD (2-hexyldecyl substitution) and L8-OD (2-octyldodecyl substitution) showed better solubility, blue-shifted absorption, upshifted LUMO energy levels, more condensed molecular stacking, and more prominent face-on orientation. However, as the branched alkyl-chain length increased, the electron mobility decreased, and the crystallization was enhanced due to interchain interaction. L8-BO showed better structural order with three π–π stacking motifs, favorable morphology and balanced charge transport, resulting in the best PCE of 18.32% with a record FF of 81.5% and an E_{loss} of 0.55 eV.

In addition to utilizing alkyl side chains to replace the n-undecyl group in Y6, some side chains with aryl groups are also widely used to optimize the structure of BT-based SMAs. In this area, Zhang and co-workers did a lot of great work. First, they changed the outer linear alkyl chains to 6-phenylhexyl and 4-hexylphenyl chains to get BTP-PhC6 and BTP-C6Ph.[83] BTP-PhC6 with bulk hexylphenyl chains showed larger steric hindrance, upshifted LUMO values, enhanced crystallinity and

Table 8 Optical, electrochemical and photovoltaic data of BT-based A–DA$_1$D–A SMAs with different side chains at the β position of the outer thiophene

SMA	$E_g^{opt\,a}$ (eV)	HOMO^b/LUMO^b (eV)	Donor	V_{OC} (V)	J_{SC} (mA cm^{-2})	FF	PCE%	Ref.
BTP-eC7	—	−5.62/−4.03	PM6	0.843	24.1	0.735	14.9	85
BTP-eC9	—	−5.64/−4.05	PM6	0.839	26.2	0.811	17.8	85
BTP-eC11	—	−5.63/−4.04	PM6	0.851	25.7	0.775	16.9	85
C5-16	—	−5.73/−3.93	PM6	0.844	27.78	0.7768	18.20	174
C6-16	—	−5.72/−3.92	PM6	0.847	27.17	0.7770	17.82	174
C7-16	—	−5.72/−3.92	PM6	0.848	26.52	0.7621	17.07	174
C8-16	—	−5.71/−3.91	PM6	0.854	26.20	0.7577	16.88	174
L8-BO	1.40	−5.68/−3.90	PM6	0.87	25.72	0.815	18.32	72
L8-HD	1.43	−5.71/−3.90	PM6	0.88	25.08	0.788	17.29	72
L8-OD	1.42	−5.71/−3.91	PM6	0.89	24.57	0.746	16.26	72
BTP-C6Ph	1.35	−5.60/−3.94	PM6	0.839	24.3	0.762	15.5	83
BTP-PhC6	1.36	−5.58/−3.85	PM6	0.865	25.0	0.77	16.7	83
o-BTP-PhC6	1.39	−5.53/−3.76	PTQ10	0.924	22.8	0.762	16.0	84
m-BTP-PhC6	1.35	−5.59/−3.86	PTQ10	0.883	25.3	0.793	17.7	84
p-BTP-PhC6	1.36	−5.59/−3.85	PTQ10	0.888	24.7	0.779	17.1	84
BTP-4F-PC6	1.37	−5.65/−3.90	PBDB-T-2F	0.855	25.08	0.8033	17.22	175
BTP-4F-P2EH	1.41	−5.65/−3.87	PBDB-T-2F	0.880	25.85	0.8008	18.22	175
BTP-4F-P3EH	1.40	−5.66/−3.89	PBDB-T-2F	0.861	26.11	0.7813	17.57	175
BTP-Th	1.34	—	PTQ10	0.878	25.2	0.762	16.8	176
BTP-FTh	1.32	−5.80/−4.04	PTQ10	0.849	26.33	0.767	17.16	62
m-TEH	1.38	−5.71/−3.92	PBQ6	0.880	26.61	0.7903	18.51	177
o-TEH	1.39	−5.70/−3.90	PBQ6	0.882	26.10	0.7042	16.22	177
BTIC-4Cl-TCl-β	1.36	−5.43/−3.89	PBDB-TF	0.86	24.30	0.7461	15.65	178
BTIC-4Cl-TCl-γ	1.35	−5.46/−3.91	PBDB-TF	0.80	23.91	0.7524	14.35	178
2-ClTh	1.41	−5.73/−4.32	D18-Cl	0.857	26.7	0.756	17.3	179
3-ClTh	1.42	−5.71/−4.29	D18-Cl	0.891	26.9	0.770	18.5	179
4-ClTh	1.44	−5.73/−4.28	D18-Cl	0.924	24.9	0.727	16.7	179
Y6-2O	1.45	−5.73/−3.76	PM6	0.92	13.3	0.535	6.6	180
Y6-1O	1.43	−5.71/−3.84	PM6	0.89	23.2	0.783	16.1	180
BTP1O-4Cl-C12	1.41	−5.84/−3.90	PM6	0.91	23.85	0.788	17.1	181
BTPS-4F	1.38	−5.73/−3.91	PM6	0.82	25.2	0.78	16.2	182
BTPS-4Cl	1.36	−5.65/−3.93	PM6	0.81	24.3	0.69	13.5	182
Y-C10ch	1.35	−5.65/−3.93	PM6	0.858	26.9	0.763	17.6	183
A-C10ch	1.38	−5.64/−3.90	PM6	0.887	26.5	0.781	18.4	183

^{a} Calculated from $E_g^{opt} = 1240/\lambda_{onset}$. ^{b} Calculated from CV curves.

This journal is © The Royal Society of Chemistry 2023
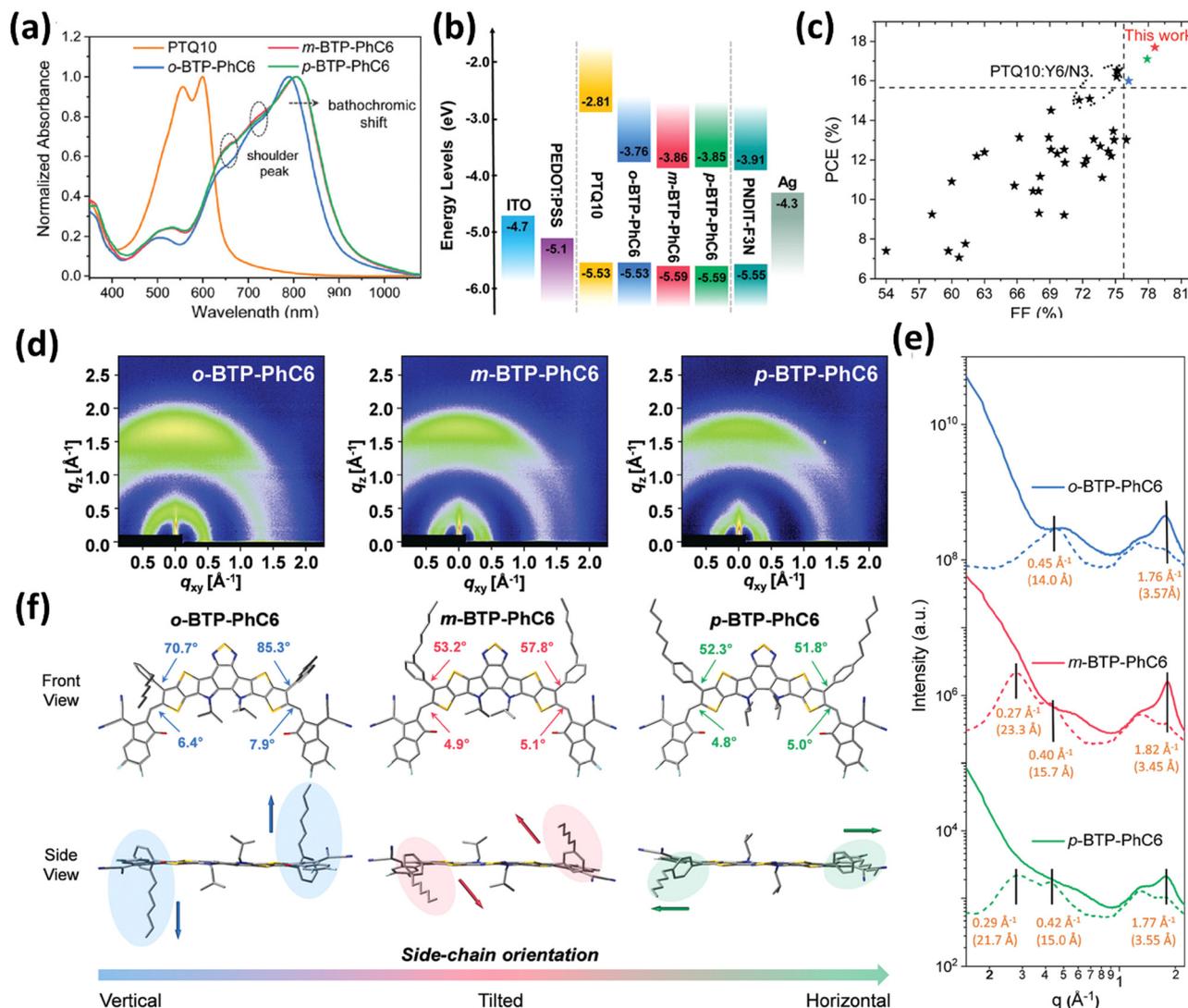
Energy Environ. Sci., 2023, **16**, 2732–2758 | **2749**

Fig. 15 (a) Normalized UV-vis absorption spectra and (b) energy level diagram of o-BTP-C6Ph, m-BTP-C6Ph and p-BTP-C6Ph; (c) comparisons of PCE and FF for PTQ10-based OSCs; (d) 2D GIWAXS patterns, (e) corresponding 1D scattering profiles and (f) DFT calculations of o-BTP-C6Ph, m-BTP-C6Ph and p-BTP-C6Ph. Adapted with permission.[84] Copyright 2021, Royal Society of Chemistry.

molecular packing, and smaller domain size in blends in comparison to BTP-C6Ph. The PM6:BTP-PhC6 device achieved a higher PCE of 16.7% than the BTP-C6Ph-based device (15.5%). Next, they adopted a strategy utilizing outer isomeric hexylphenyl side chains for high performance OSCs.[84] Because of the steric hindrance effect, the outer side chain in o-BTP-PhC6 with ortho-substitution position presents a vertical orientation, while p-BTP-PhC6 with para-substituted chains presents a horizontal orientation, and m-BTP-PhC6 with meta-substituted chains shows a "tilted" orientation (Fig. 15). Compared to p-BTP-C6Ph and m-BTP-PhC6, o-BTP-PhC6 demonstrates blue-shifted absorption spectra and a shallower LUMO value because of the low degree of molecular aggregation. As a result, m-BTP-PhC6 displays the best intermolecular π–π stacking. The device based on m-BTP-C6Ph and low-cost PTQ10 achieved the best efficiency of 17.7% in comparison to PTQ10:o-BTP-C6Ph (16.0%) and PTQ10:p-BTP-C6Ph (17.1%) devices, resulting from

an appropriate phase separation, improved molecular stacking and more ordered side-chain orientations. Then, they changed the outer linear m-hexylphenyl chains to γ-branched BTP-4F-P3EH and β-branched BTP-4F-P2EH.[175] BTP-4F-P2EH and BTP-4F-P3EH exhibited better solubility, slightly blue-shifted absorption and upshifted LUMOs, and suitable domain size in blends compared with p-BTP-C6Ph. BTP-4F-P2EH and BTP-4F-P3EH-based devices achieve enhanced V_{OC} due to reduced non-radiative voltage losses, resulting in superior PCEs of 18.22% and 17.57%, respectively. Additionally, they replaced the outer 4-hexylphenyl alkyl side chains of BTP-PhC6 with 5-octylthienyl (BTP-Th), and a similar PCE of 16.8% was achieved for the PTQ10:BTP-Th device.[176] Recently, Li et al. adopted a strategy of using thiophene outer side chains with branched 2-ethylhexyl-substituted at α- or β-position to get two isomeric SMAs, namely o-THE and m-TEH.[177] The 2-ethylhexyl substitution position has a negligible effect on their optical and electrochemical properties; however, m-TEH

2750 | Energy Environ. Sci., 2023, 16, 2732–2758

This journal is © The Royal Society of Chemistry 2023

presents reinforced molecular π–π stacking and enhanced charge mobility due to smaller steric hindrance. The PBQ6:*m*-TEH device achieved a better efficiency of 18.51% compared to the *o*-THE-based device (16.22%).

Introducing a halogen into thiophene side chains of SMAs is an important means to enhance intermolecular forces and improve photovoltaic performance. Peng *et al.* synthesized BTP-FTh with β-fluorination of outer thiophene side chains.[62] Compared with non-fluorinated BTP-Th, BTP-FTh exhibited slightly redshifted absorption, higher absorption coefficients, downshifted energy levels, higher crystallinity and electron mobility, thereby resulting in a higher PCE of 17.16% in the PTQ10:BTP-FTh device. He *et al.* investigated the chlorination effect in outer thiophene side chains. Compared with non-chlorinated BTIC-4Cl-T, BTIC-4Cl-TCl-β with chlorination at β position displayed obviously blue-shifted absorption, and BTIC-4Cl-TCl-γ with chlorination at γ position presented slightly blue-shifted absorption.[178] Chlorination had little impact on energy levels. Additionally, the single crystal structure indicates that BTIC-4Cl-TCl-β exhibits a twisty skeleton due to large steric hindrance effects, resulting in the presence of only *J*-aggregation in the BTIC-4Cl-TCl-β quasi-3D network. BTIC-4Cl-TCl-γ can form both *J*-aggregation and *H*–aggregation 3D networks due to a highly planar structure. BTIC-4Cl-TCl-β-based cells achieved a PCE of 15.65% and the BTIC-4Cl-TCl-γ-based device achieved a PCE of 14.35%, which are much better than that of the BTIC-4Cl-T-based device (10.86%). Furthermore, Jen and co-workers reported three isomeric SMAs by changing the position of chlorine and 2-butyloctyl in thienyl side chains, namely, 2-ClTh, 3-ClTh, and 4-ClTh.[179]

The 3-ClTh isomer showed balanced end- and side-group torsion angles relative to those of 2-ClTh and 4-ClTh, which

endowed 3-ClTh with a higher PCE of 18.5% along with a lower energy loss of 0.528 V.

Heteroatoms, such as O and S, were incorporated into the outer side chains of BT-based A–DA₁D–A type SMAs. For example, Yan *et al.* modified the two outer side chains to get Y6-2O with alkoxy chains and Y6-1O with asymmetric alkoxy and alkyl chains.[180] Because of the conformational-locking role of the alkoxy chains, Y6-2O showed poor solubility and excessive aggregation. Compared with Y6, alkoxy chains endow Y6-1O and Y6-2O relatively blue-shifted absorption spectra, elevated LUMO values and almost unchanged HOMO energy levels. The PM6:Y6-1O device delivered a high efficiency of 16.1%, and the PM6:Y6-1O:PC₇₁BM ternary device showed a PCE of 17.6%. Based on the outer asymmetric alkoxy and alkyl side chains and chlorine-substitution strategies, the same group adopted inner side chain engineering to improve photovoltaic performance.[181] BTP1O-4Cl-C12 exhibited good solubility and favorable morphology characterization, and the PM6:BTP1O-4Cl-C12 blend achieved an outstanding efficiency of 17.1%. Furthermore, they replaced the outer alkyl chains of Y6 with alkylthio chains to get BTPS-4F and BTPS-4Cl.[182] BTPS-4Cl showed redshifted absorption and enhanced absorption ability, upshifted HOMO values, but weaker molecular π–π packing in comparison to BTPS-4F. The PM6:BTPS-4F device delivered a higher PCE of 16.2% than the PM6:BTPS-4Cl device (13.5%).

Cycloalkyl–alkyl chains were used to develop symmetric/asymmetric SMAs, namely, Y-C10ch and A-C10ch. Compared to L8-BO, the cyclohexyldecyl chain in Y-C10ch and A-C10ch leads to a more planar backbone and tighter 3D network stacking, resulting in the better domain purity. As a result, the asymmetric A-C10ch achieved the best PCE of 18.4% due to its balanced V_{OC}, J_{SC} and FF values.[183]

Fig. 16 Chemical structures of BTA-based SMAs with different side chains.

This journal is © The Royal Society of Chemistry 2023

Energy Environ. Sci., 2023, **16**, 2732–2758 | **2751**

Table 9 Optical, electrochemical and photovoltaic data of BTA-based A–DA$_1$D–A SMAs with different side chains

SMA	$E_g^{opt\,a}$ (eV)	HOMO^b/LUMO^b (eV)	Donor	V_{OC} (V)	J_{SC} (mA cm^{-2})	FF	PCE%	Ref.
Y11	1.30	−5.65/−3.90	PM6	0.87	23.69	0.720	14.85	184
Y11-M	1.30	−5.60/−3.96	PM6	0.86	25.54	0.7615	16.64	184
Y11-EB	1.30	−5.59/−3.95	PM6	0.88	26.20	0.7473	17.15	184
BTA-C1	—	−5.64/−3.99	PM6	0.844	24.75	0.7762	16.21	185
BTA-C5	—	−5.66/−4.00	PM6	0.847	26.51	0.7619	17.11	185
BTA-C6	—	−5.65/−3.97	PM6	0.851	25.20	0.7568	16.23	185
BTA-C8	—	−5.66/−3.96	PM6	0.837	26.18	0.7567	16.59	185
mBzS-4F	1.25	−5.60/−3.90	PM6	0.804	27.72	0.7635	17.02	186
EHBzS-4F	1.24	−5.61/−3.86	PM6	0.825	27.58	0.7007	15.94	186
PN6SBO-4F	1.28	−5.63/−3.87	PM6	0.825	23.12	0.6665	12.73	187
AN6SBO-4F	1.27	−5.60/−3.88	PM6	0.822	16.06	0.6298	8.32	187
EHN6SEH-4F	1.29	−5.59/−3.89	PM6	0.809	28.83	0.7464	17.48	187

^{a} Calculated from $E_g^{opt} = 1240/\lambda_{onset}$. ^{b} Calculated from CV curves.

3.2. Side-chain engineering of BTA-based SMAs

In comparison with BT-based SMAs, benzo[2,1,3]triazole (BTA)-based SMAs have one more side chain due to the introduction of an additional nitrogen atom. Modifying the N alkyl chain of BTA plays a vital role in promoting cell efficiency. Zou *et al.* replaced the 2-ethylhexyl chains in the BTA unit with methyl groups for Y11-M and the 2-ethylhexyl chains in the pyrrole ring with 2-ethylbutyl chains for Y11-EB.[184] In comparison with Y11, Y11-EB and Y11-M exhibited intense absorption in the wavelength range from 450 to 850 nm and narrow bandgaps due to smaller steric hindrance (Fig. 16). PM6:Y11-EB and PM6:Y11-M devices achieved better PCEs of 17.15% and 16.64% (Table 9), respectively. They also systematically investigated the impact of alkyl side chain length in the BTA unit of BTA-C8 (Y18).[185] BTA-C1 and BTA-C6 with linear chains showed lower solubility and excessive aggregation. BTA-C5 with shorter 2-methylbutyl branched chains presented suitable solubility and enhanced crystallinity. The PCEs of the four devices were over 16%, and PM6:BTA-C5 achieved the highest PCE of 17.11%.

K.-Y. Jen exploited a series of Se-substituted BTA-based SMAs, and systematically investigated the effects of alkyl chains on nitrogen of BTA-based SMAs on molecular packing and device performance. First, they replaced the 2-ethylhexyl in the BTA unit of selenophene-fused EHBzS-4F with a methyl group to get mBzS-4F. Compared with EHBzS-4F, mBzS-4F delivered intense absorption in the 300–900 nm region in films, downshifted LUMO values, stronger π–π interaction and favorable crystallinity. The device based on mBzS-4F achieved an efficiency of 17.02% as well as a high J_{SC} (27.72 mA cm^{-2}), which are better than those of the EHBzS-4F-based device (PCE = 15.94% and J_{SC} = 27.58 mA cm^{-2}).[186] Furthermore, they replaced 2-butyloctyl in EHBzS-4F with 2-ethylhexyl to develop EHN6SEH-4F, and a better PCE of 17.48% was achieved, originating from the effective charge-transporting behaviors in 3D networks.[187]

4. Conclusion and outlook

Side-chain engineering is of significant importance for developing high-performance nonfullerene SMAs in the field of OSCs. Side chains of SMAs not only act as soluble groups, but also have an important influence on interchain/intermolecular stacking properties and the photoelectric efficiency of the resulting SMAs. To date, binary OSCs based on newly reported SMAs *via* side chain optimization have achieved PCEs of over 18%. Despite this good progress, some aspects require further research, such as the design and synthesis of novel small-molecule electron acceptors with some specific side chains, and the systematic investigation of the relationship among structure, morphology, performance, and stability. For future development of side-chain engineering in SMAs, the following research guidelines are worth considering from the perspective of molecular design.

(1) Developing SMAs with hydrogen-bond-assisted molecular packing *via* aryl side chains. Very recently, our group demonstrated that BTP-PhC6 with 3-hexylphenyl side chains shows hydrogen-bond-assisted 3D network packing; however, there is no intermolecular hydrogen bond in the 3D crystal stacking of Y6 (Fig. 17). Compared with Y6, hydrogen bonds endow BTP-PhC6 with enhanced π···π stacking between two close end groups and larger electronic coupling, thus resulting in better FF and PCE in BTP-PhC6-based devices.[82] With Y6 and BTP-PhC6 as parent acceptors, we developed an asymmetric acceptor (BTP-PhC6-C11) by replacing one side chain on thiophene of Y6 with 3-hexylphenyl in BTP-PhC6. Thanks to the synergistic impact of small torsion angles (originated from Y6) and hydrogen-bond interactions (originated from BTP-PhC6), the asymmetric acceptor exhibited the closest π···π packing between two end groups and a more obvious (001) diffraction signal in the IP direction, contributing to the charge transport along molecular backbones of the asymmetric acceptor. Finally, the OSCs based on the asymmetric acceptor BTP-PhC6-C11 yielded a distinguished efficiency of 18.33%.

(2) Developing SMAs with nitrogen-containing side chains. The nitrogen atom in the diphenylamine side chains can form an N···S conformational lock with the S atom on the adjacent thiophene, which can improve the planarity of the molecule, thereby increasing the electron mobility of the acceptors. Therefore, choosing suitable nitrogen-containing side chains is a good method to boost the photovoltaic performance.

(3) Developing SMAs containing functional groups (hydroxyl, acetoxy groups, carboxyl, *etc.*) in side chains. He *et al.* reported a
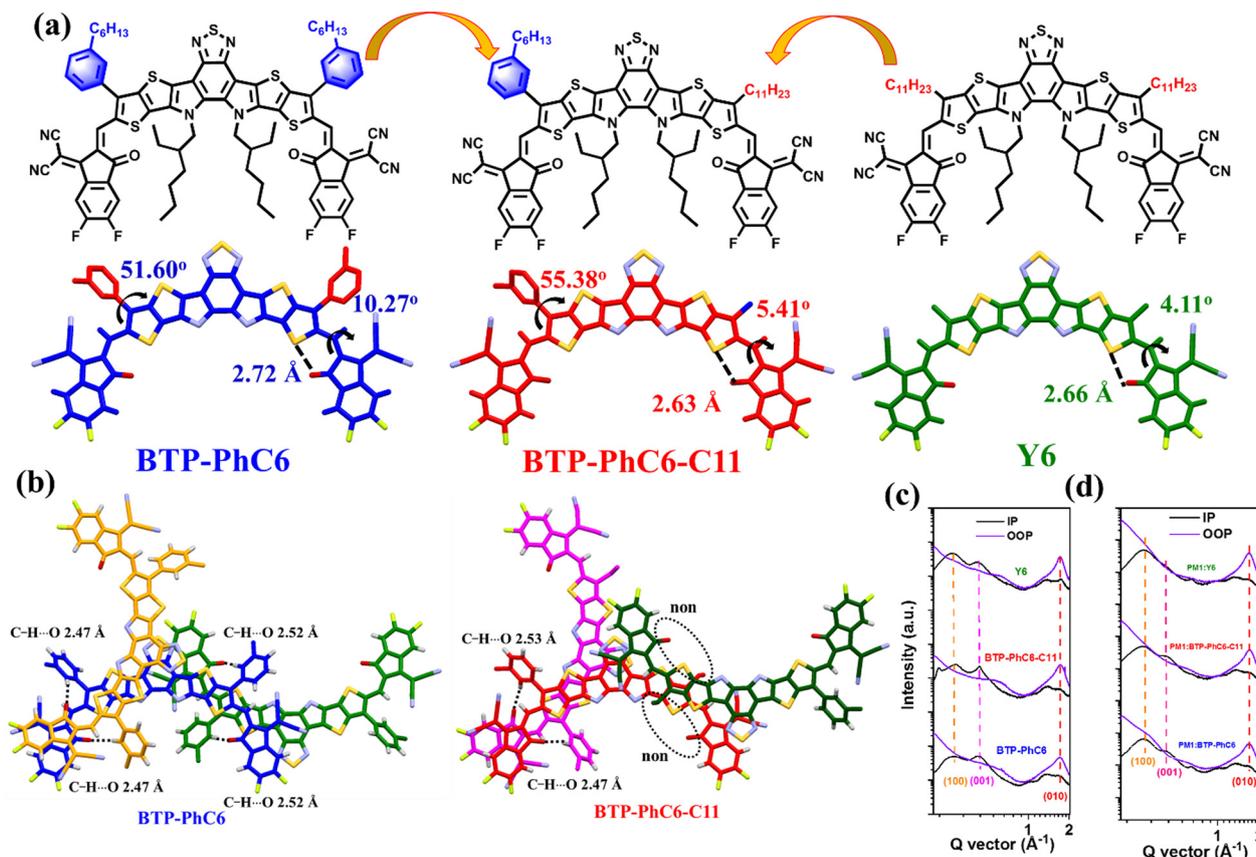
Fig. 17 (a) Molecular and monomolecular single crystallographic structures of asymmetric BTP-PhC6-C11, and symmetric Y6, and BTP-PhC6; (b) hydrogen bonding interactions of C−H···O in BTP-PhC6-C11 and BTP-PhC6; the IP and OOP line-cut profiles of (c) neat BTP-PhC6-C11, Y6, BTP-PhC6 films and (d) PM1:acceptor blends. Adapted with permission.[82] Copyright 2022, Royal Society of Chemistry.

polymer donor NTI-OAc with acetoxy groups as the terminal units of the side chains.[188] NTI-OAc-based quasiplanar heterojunction OSCs realized high device efficiency (16.53%) and quite superior device stability.

(4) Developing SMAs with more π–π packing motifs. Optimizing side chains can increase the number of π–π packing motifs in the resulting SMAs, creating additional charge-hopping pathways, thereby resulting in better molecular packing in films and enhanced charge mobility.

(5) Developing non-fused-ring SMAs with bulky side chains. The bulky side chains can usually make the central core of non-fused-ring SMAs smoother due to the effect of steric hindrance, which is beneficial to the electron transport and the intermolecular packing between two central cores. While for fused-ring SMAs, large steric side chains are unfavorable for molecular stacking between two end groups.

(6) Developing SMAs with a suitable length of alkyl side chains. When the alkyl chains are too short, the SMAs can have poor solubility and be challenging to process in solution. On the other hand, if the alkyl chains are too long, the material can be prone to crystallization, leading to significant phase separation between the donor and the acceptor components.[72] Recently, Tang and co-workers found that longer side chains in SMAs are beneficial in reducing non-radiative recombination

loss and increasing the V_{OC} of the device without affecting the dissociation efficiency of the excitons, implying the importance of longer side chains in developing high-performance SMAs.[189] Therefore, it is essential to find a balance in the length of the alkyl chains to optimize the material's solubility and crystallization/aggregation behavior.

Overall, side-chain engineering is a useful, important and convenient approach to optimize the chemical structure of small-molecule acceptors, so as to realize organic photovoltaic devices with high efficiency and good stability. We believe that evolving SMAs through side-chain engineering, together with innovations in donor materials, device process optimization, interface selection, and packaging technology improvements, will bring us closer to the commercialization of organic solar cells.

Conflicts of interest

There are no conflicts to declare.

Acknowledgements

References

1 P. Cheng and X. Zhan, *Chem. Soc. Rev.*, 2016, **45**, 2544.

2 J. Zhang, H. S. Tan, X. Guo, A. Facchetti and H. Yan, *Nat. Energy*, 2018, **3**, 720.

3 X. Wan, C. Li, M. Zhang and Y. Chen, *Chem. Soc. Rev.*, 2020, **49**, 2828.

4 Y. Lin and X. Zhan, *Acc. Chem. Res.*, 2016, **49**, 175.

5 J. Wang, P. Xue, Y. Jiang, Y. Huo and X. Zhan, *Nat. Rev. Chem.*, 2022, **6**, 614.

6 G. Zhang, F. R. Lin, F. Qi, T. Heumüller, A. Distler, H.-J. Egelhaaf, N. Li, P. C. Y. Chow, C. J. Brabec, A. K.-Y. Jen and H.-L. Yip, *Chem. Rev.*, 2022, **122**, 14180.

7 J. Hou, O. Inganas, R. H. Friend and F. Gao, *Nat. Mater.*, 2018, **17**, 119.

8 L. Ye, H. Hu, M. Ghasemi, T. Wang, B. A. Collins, J.-H. Kim, K. Jiang, J. H. Carpenter, H. Li, Z. Li, T. McAfee, J. Zhao, X. Chen, J. L. Y. Lai, T. Ma, J.-L. Bredas, H. Yan and H. Ade, *Nat. Mater.*, 2018, **17**, 253.

9 Y. Lin, J. Wang, Z.-G. Zhang, H. Bai, Y. Li, D. Zhu and X. Zhan, *Adv. Mater.*, 2015, **27**, 1170.

10 J. Yuan, Y. Zhang, L. Zhou, G. Zhang, H.-L. Yip, T.-K. Lau, X. Lu, C. Zhu, H. Peng, P. A. Johnson, Y. Li and Y. Zou, *Joule*, 2019, **3**, 1140.

11 J. Yuan, T. Huang, P. Cheng, Y. Zou, H. Zhang, J. L. Yang, S.-Y. Chang, Z. Zhang, W. Huang, R. Wang, D. Meng, F. Gao and Y. Yang, *Nat. Commun.*, 2019, **10**, 570.

12 Y. Li, *Acc. Chem. Res.*, 2012, **45**, 723.

13 T. Xu, J. Lv, K. Yang, Y. He, Q. Yang, H. Chen, Q. Chen, Z. Liao, Z. Kan, T. Duan, K. Sun, J. Ouyang and S. Lu, *Energy Environ. Sci.*, 2021, **14**, 5366.

14 Y. Liu, B. Liu, C.-Q. Ma, F. Huang, G. Feng, H. Chen, J. Hou, L. Yan, Q. Wei, Q. Luo, Q. Bao, W. Ma, W. Liu, W. Li, X. Wan, X. Hu, Y. Han, Y. Li, Y. Zhou, Y. Zou, Y. Chen, Y. Li, Y. Chen, Z. Tang, Z. Hu, Z.-G. Zhang and Z. Bo, *Sci. China Chem.*, 2022, **65**, 224.

15 Q. Bai, Q. Liang, H. Li, H. Sun, X. Guo and L. Niu, *Aggregate*, 2022, **3**, e281.

16 C.-Y. Liao, Y. Chen, C.-C. Lee, G. Wang, N.-W. Teng, C.-H. Lee, W.-L. Li, Y.-K. Chen, C.-H. Li, H.-L. Ho, P. H.-S. Tan, B. Wang, Y.-C. Huang, R. M. Young, M. R. Wasielewski, T. J. Marks, Y.-M. Chang and A. Facchetti, *Joule*, 2020, **4**, 189.

17 S. Li, L. Zhan, Y. Jin, G. Zhou, T.-K. Lau, R. Qin, M. Shi, C.-Z. Li, H. Zhu, X. Lu, F. Zhang and H. Chen, *Adv. Mater.*, 2020, **32**, 2001160.

18 Y. Zhang, Y. Ji, Y. Zhang, W. Zhang, H. Bai, M. Du, H. Wu, Q. Guo and E. Zhou, *Adv. Funct. Mater.*, 2022, **32**, 2205115.

19 B. Li, X. Zhang, Z. Wu, J. Yang, B. Liu, Q. Liao, J. Wang, K. Feng, R. Chen, H. Y. Woo, F. Ye, L. Niu, X. Guo and H. Sun, *Sci. China Chem*, 2022, **65**, 1157.

20 Z. Luo, R. Ma, J. Yu, H. Liu, T. Liu, F. Ni, J. Hu, Y. Zou, A. Zeng, C.-J. Su, U.-S. Jeng, X. Lu, F. Gao, C. Yang and H. Yan, *Natl. Sci. Rev.*, 2022, **9**, nwac076.

21 Z. Xiao, S. Yang, Z. Yang, J. Yang, H. L. Yip, F. Zhang, F. He, T. Wang, J. Wang, Y. Yuan, H. Yang, M. Wang and L. Ding, *Adv. Mater.*, 2019, **31**, 1804790.

22 X. Gu, J. Gao, Z. Han, Y. Shi, Y. Wei, Y. Zhang, Q. Peng, Z. Wei, X. Zhang and H. Huang, *Chin. J. Polym. Sci.*, 2023, **41**, 556.

23 L. Meng, Y. Zhang, X. Wan, C. Li, X. Zhang, Y. Wang, X. Ke, Z. Xiao, L. Ding, R. Xia, H.-L. Yip, Y. Cao and Y. Chen, *Science*, 2018, **361**, 1094.

24 R. Ma, C. Yan, J. Yu, T. Liu, H. Liu, Y. Li, J. Chen, Z. Luo, B. Tang, X. Lu, G. Li and H. Yan, *ACS Energy Lett*, 2022, **7**, 2547.

25 W. Gao, F. Qi, Z. Peng, F. R. Lin, K. Jiang, C. Zhong, W. Kaminsky, Z. Guan, C. S. Lee, T. J. Marks, H. Ade and A. K. Jen, *Adv. Mater.*, 2022, **34**, 2202089.

26 B. Fan, D. Zhang, M. Li, W. Zhong, Z. Zeng, L. Ying, F. Huang and Y. Cao, *Sci. China: Chem.*, 2019, **62**, 746.

27 Z. Luo, T. Liu, J. Oh, R. Ma, J. Miao, F. Ni, G. Zhang, R. Sun, C. Zhang, Z. Chen, Y. Zou, J. Min, C. Yang, H. Yan and C. Yang, *Adv. Funct. Mater.*, 2022, **32**, 2203200.

28 H. B. Naveed and W. Ma, *Joule*, 2018, **2**, 621.

29 O. V. Mikhnenko, P. W. M. Blom and T.-Q. Nguyen, *Energy Environ. Sci.*, 2015, **8**, 1867.

30 H. Lai, Q. Zhao, Z. Chen, H. Chen, P. Chao, Y. Zhu, Y. Lang, N. Zhen, D. Mo, Y. Zhang and F. He, *Joule*, 2020, **4**, 688.

31 R. Ma, C. Yan, P. W.-K. Fong, J. Yu, H. Liu, J. Yin, J. Huang, X. Lu, H. Yan and G. Li, *Energy Environ. Sci.*, 2022, **15**, 2479.

32 Z. Zhou, S. Xu, J. Song, Y. Jin, Q. Yue, Y. Qian, F. Liu, F. Zhang and X. Zhu, *Nat. Energy*, 2018, **3**, 952.

33 Z. Zhang, Y. Li, G. Cai, Y. Zhang, X. Lu and Y. Lin, *J. Am. Chem. Soc.*, 2020, **142**, 18741.

34 N. Gasparini, M. Salvador, S. Strohm, T. Heumueller, I. Levchuk, A. Wadsworth, J. H. Bannock, J. C. de Mello, H. J. Egelhaaf, D. Baran, I. McCulloch and C. J. Brabec, *Adv. Energy Mater*, 2017, **7**, 1700770.

35 Y. Jiang, X. Dong, L. Sun, T. Liu, F. Qin, C. Xie, P. Jiang, L. Hu, X. Lu, X. Zhou, W. Meng, N. Li, C. J. Brabec and Y. Zhou, *Nat. Energy*, 2022, **7**, 352.

36 R. Ma, K. Zhou, Y. Sun, T. Liu, Y. Kan, Y. Xiao, T. A. D. Peña, Y. Li, X. Zou, Z. Xing, Z. Luo, K. S. Wong, X. Lu, L. Ye, H. Yan and K. Gao, *Matter*, 2022, **5**, 725.

37 Z. Luo, T. Liu, H. Yan, Y. Zou and C. Yang, *Adv. Funct. Mater.*, 2020, **30**, 2004477.

38 C. Yan, J. Qin, Y. Wang, G. Li and P. Cheng, *Adv. Energy Mater*, 2022, **12**, 2201087.

39 Q. Fan, R. Ma, W. Su, Q. Zhu, Z. Luo, K. Chen, Y. Tang, F. Lin, Y. Li, H. Yan, C. Yang, A. K. Jen and W. Ma, *Carbon Energy*, 2022, **5**, e267.

40 Z. Luo, T. Liu, R. Ma, Y. Xiao, L. Zhan, G. Zhang, H. Sun, F. Ni, G. Chai, J. Wang, C. Zhong, Y. Zou, X. Guo, X. Lu, H. Chen, H. Yan and C. Yang, *Adv. Mater.*, 2020, **32**, 2005942.

41 Y. Li, J. D. Lin, X. Che, Y. Qu, F. Liu, L. S. Liao and S. R. Forrest, *J. Am. Chem. Soc.*, 2017, **139**, 17114.

42 L. Yan, H. Zhang, Q. An, M. Jiang, A. Mahmood, M. H. Jee, H.-R. Bai, H.-F. Zhi, S. Zhang, H. Y. Woo and J.-L. Wang, *Angew. Chem., Int. Ed.*, 2022, **134**, e202209454.

43 H. Sun, X. Guo and A. Facchetti, *Chem*, 2020, **6**, 1310.

2754 | *Energy Environ. Sci.*, 2023, **16**, 2732–2758

This journal is © The Royal Society of Chemistry 2023

44 Z. Luo, R. Ma, Z. Chen, Y. Xiao, G. Zhang, T. Liu, R. Sun, Q. Zhan, Y. Zou, C. Zhong, Y. Chen, H. Sun, G. Chai, K. Chen, X. Guo, J. Min, X. Lu, C. Yang and H. Yan, *Adv. Energy Mater.*, 2020, **10**, 2002649.

45 C. Yan, S. Barlow, Z. Wang, H. Yan, A. K. Y. Jen, S. R. Marder and X. Zhan, *Nat. Rev. Mater*, 2018, **3**, 18003.

46 G. Zhang, J. Zhao, P. C. Y. Chow, K. Jiang, J. Zhang, Z. Zhu, J. Zhang, F. Huang and H. Yan, *Chem. Rev.*, 2018, **118**, 3447.

47 X. Li, F. Pan, C. Sun, M. Zhang, Z. Wang, J. Du, J. Wang, M. Xiao, L. Xue, Z. G. Zhang, C. Zhang, F. Liu and Y. Li, *Nat. Commun.*, 2019, **10**, 519.

48 Z. Luo, T. Liu, Y. Wang, G. Zhang, R. Sun, Z. Chen, C. Zhong, J. Wu, Y. Chen, M. Zhang, Y. Li and C. Yang, *Adv. Energy Mater.*, 2019, **9**, 1900041.

49 V. Coropceanu, X.-K. Chen, T. Wang, Z. Zheng and J.-L. Brédas, *Nat. Rev. Mater.*, 2019, **4**, 689.

50 G. J. Hedley, A. Ruseckas and I. D. Samuel, *Chem. Rev.*, 2017, **117**, 796.

51 K. Feng, H. Guo, J. Wang, Y. Shi, Z. Wu, M. Su, X. Zhang, J. H. Son, H. Y. Woo and X. Guo, *J. Am. Chem. Soc.*, 2021, **143**, 1539.

52 J. Yan, X. Rodrıguez-Martınez, D. Pearce, H. Douglas, D. Bili, M. Azzouzi, F. Eisner, A. Virbule, E. Rezasoltani, V. Belova, B. Dorling, S. Few, A. A. Szumska, X. Hou, G. Zhang, H. Lap Yip, M. Campoy-Quiles and J. Nelson, *Energy Environ. Sci.*, 2022, **15**, 2958.

53 Y. Shi, Y. Chang, K. Lu, Z. Chen, J. Zhang, Y. Yan, D. Qiu, Y. Liu, M. A. Adil, W. Ma, X. Hao, L. Zhu and Z. Wei, *Nat. Commun.*, 2022, **13**, 3256.

54 T. Xu, J. Lv, Z. Chen, Z. Luo, G. Zhang, H. Liu, H. Huang, D. Hu, X. Lu, S. Lu and C. Yang, *Adv. Funct. Mater.*, 2022, **33**, 2210549.

55 H. Lai, H. Chen, J. Zhou, J. Qu, P. Chao, T. Liu, X. Chang, N. Zheng, Z. Xie and F. He, *iScience*, 2019, **17**, 302.

56 C. Lee, S. Lee, G. U. Kim, W. Lee and B. J. Kim, *Chem. Rev.*, 2019, **119**, 8028.

57 X. Xu, Y. Li and Q. Peng, *Adv. Mater.*, 2022, **34**, 2107476.

58 J. Xu, S. B. Jo, X. Chen, G. Zhou, M. Zhang, X. Shi, F. Lin, L. Zhu, T. Hao, K. Gao, Y. Zou, X. Su, W. Feng, A. K.-Y. Jen, Y. Zhang and F. Liu, *Adv. Mater.*, 2022, **34**, 2108317.

59 K.-N. Zhang, X.-Y. Du, Z.-H. Chen, T. Wang, Z.-Q. Yang, H. Yin, Y. Yang, W. Qin and X.-T. Hao, *Adv. Energy Mater.*, 2022, **12**, 2103371.

60 M. Jiang, H.-F. Zhi, B. Zhang, C. Yang, A. Mahmood, M. Zhang, H. Y. Woo, F. Zhang, J.-L. Wang and Q. An, *ACS Energy Lett.*, 2023, **8**, 1058.

61 A. Classen, C. L. Chochos, L. Lüer, V. G. Gregoriou, J. Wortmann, A. Osvet, K. Forberich, I. McCulloch, T. Heumüller and C. J. Brabec, *Nat. Energy*, 2020, **5**, 711.

62 K. Chong, X. Xu, H. Meng, J. Xue, L. Yu, W. Ma and Q. Peng, *Adv. Mater.*, 2022, **34**, 2109516.

63 Y. Cui, Y. Xu, H. Yao, P. Bi, L. Hong, J. Zhang, Y. Zu, T. Zhang, J. Qin, J. Ren, Z. Chen, C. He, X. Hao, Z. Wei and J. Hou, *Adv. Mater.*, 2021, **33**, 2102420.

64 L. Zhu, M. Zhang, J. Xu, C. Li, J. Yan, G. Zhou, W. Zhong, T. Hao, J. Song, X. Xue, Z. Zhou, R. Zeng, H. Zhu,

C.-C. Chen, R. C. I. MacKenzie, Y. Zou, J. Nelson, Y. Zhang, Y. Sun and F. Liu, *Nat. Mater.*, 2022, **21**, 656.

65 C. He, Y. Pan, Y. Ouyang, Q. Shen, Y. Gao, K. Yan, J. Fang, Y. Chen, C.-Q. Ma, J. Min, C. Zhang, L. Zuo and H. Chen, *Energy Environ. Sci.*, 2022, **15**, 2537.

66 L. Zuo, S. B. Jo, Y. Li, Y. Meng, R. J. Stoddard, Y. Liu, F. Lin, X. Shi, F. Liu, H. W. Hillhouse, D. S. Ginger, H. Chen and A. K. Y. Jen, *Nat. Nanotechnol.*, 2022, **17**, 53.

67 F. Eisner and J. Nelson, *Joule*, 2021, **5**, 1319.

68 M. Moser, A. Wadsworth, N. Gasparini and I. McCulloch, *Adv. Energy Mater.*, 2021, **11**, 2100056.

69 G. Bernardo, T. Lopes, D. G. Lidzey and A. Mendes, *Adv. Energy Mater.*, 2021, **11**, 2100342.

70 T. Liu, K. Zhou, R. Ma, L. Zhang, C. Huang, Z. Luo, H. Zhu, S. Yao, C. Yang, B. Zou and L. Ye, *Aggregate*, 2023, **4**, e308.

71 T. Wang, G. Kupgan and J.-L. Brédas, *Trends Chem.*, 2020, **2**, 535.

72 C. Li, J. Zhou, J. Song, J. Xu, H. Zhang, X. Zhang, J. Guo, L. Zhu, D. Wei, G. Han, J. Min, Y. Zhang, Z. Xie, Y. Yi, H. Yan, F. Gao, F. Liu and Y. Sun, *Nat. Energy*, 2021, **6**, 605.

73 L. Zhan, S. Li, Y. Li, R. Sun, J. Min, Y. Chen, J. Fang, C.-Q. Ma, G. Zhou, H. Zhu, L. Zuo, H. Qiu, S. Yin and H. Chen, *Adv. Energy Mater.*, 2022, **12**, 2201076.

74 Z. Chen, X. Chen, Z. Jia, G. Zhou, J. Xu, Y. Wu, X. Xia, X. Li, X. Zhang, C. Deng, Y. Zhang, X. Lu, W. Liu, C. Zhang, Y. Yang and H. Zhu, *Joule*, 2021, **5**, 1832.

75 X. Xia, T.-K. Lau, X. Guo, Y. Li, M. Qin, K. Liu, Z. Chen, X. Zhan, Y. Xiao, P. F. Chan, H. Liu, L. Xu, G. Cai, N. Li, H. Zhu, G. Li, Y. Zhu, T. Zhu, X. Zhan, X.-L. Wang and X. Lu, *Nat. Commun.*, 2021, **12**, 6226.

76 T. P. Chaney, A. J. Levin, S. A. Schneider and M. F. Toney, *Mater. Horiz.*, 2022, **9**, 43.

77 S. Liu, J. Yuan, W. Deng, M. Luo, Y. Xie, Q. Liang, Y. Zou, Z. He, H. Wu and Y. Cao, *Nat. Photonics*, 2020, **14**, 300.

78 T. Liu, R. Ma, Z. Luo, Y. Guo, G. Zhang, Y. Xiao, T. Yang, Y. Chen, G. Li, Y. Yi, X. Lu, H. Yan and B. Tang, *Energy Environ. Sci.*, 2020, **13**, 2115.

79 L. Zhan, S. Yin, Y. Li, S. Li, T. Chen, R. Sun, J. Min, G. Zhou, H. Zhu, Y. Chen, J. Fang, C.-Q. Ma, X. Xia, X. Lu, H. Qiu, W. Fu and H. Chen, *Adv. Mater.*, 2022, **34**, 2206269.

80 R. Sun, Y. Wu, X. Yang, Y. Gao, Z. Chen, K. Li, J. Qiao, T. Wang, J. Guo, C. Liu, X. Hao, H. Zhu and J. Min, *Adv. Mater.*, 2022, **34**, 2110147.

81 Y. Wei, Z. Chen, G. Lu, N. Yu, C. Li, J. Gao, X. Gu, X. Hao, G. Lu, Z. Tang, J. Zhang, Z. Wei, X. Zhang and H. Huang, *Adv. Mater.*, 2022, **34**, 2204718.

82 Z. Luo, Y. Gao, H. Lai, Y. Li, Z. Wu, Z. Chen, R. Sun, J. Ren, C. Zhang, F. He, H. Woo, J. Min and C. Yang, *Energy Environ. Sci.*, 2022, **15**, 4601.

83 G. Chai, Y. Chang, Z. Peng, Y. Jia, X. Zou, D. Yu, H. Yu, Y. Chen, P. C. Y. Chow, K. S. Wong, J. Zhang, H. Ade, L. Yang and C. Zhan, *Nano Energy*, 2020, **76**, 105807.

84 G. Chai, Y. Chang, J. Zhang, X. Xu, L. Yu, X. Zou, X. Li, Y. Chen, S. Luo, B. Liu, F. Bai, Z. Luo, H. Yu, J. Liang, T. Liu, K. S. Wong, H. Zhou, Q. Peng and H. Yan, *Energy Environ. Sci.*, 2021, **14**, 3469.

This journal is © The Royal Society of Chemistry 2023

Energy Environ. Sci., 2023, **16**, 2732–2758 | **2755**

85 Y. Cui, H. Yao, J. Zhang, K. Xian, T. Zhang, L. Hong, Y. Wang, Y. Xu, K. Ma, C. An, C. He, Z. Wei, F. Gao and J. Hou, *Adv. Mater.*, 2020, **32**, 1908205.

86 C. Li, H. Fu, T. Xia and Y. Sun, *Adv. Energy Mater.*, 2019, **9**, 1900999.

87 D. Li, C. Sun, T. Yan, J. Yuan and Y. Zou, *ACS Cent. Sci.*, 2021, **7**, 1787.

88 J. Huang, H. Tang, C. Yan and G. Li, *Cell Rep. Phys. Sci.*, 2021, **2**, 100292.

89 S. Suman and S. P. Singh, *J. Mater. Chem. A*, 2019, **7**, 22701.

90 Z.-Q. Jiang, T.-T. Wang, F.-P. Wu, J.-D. Lin and L.-S. Liao, *J. Mater. Chem. A*, 2018, **6**, 17256.

91 F. Shen, J. Xu, X. Li and C. Zhan, *J. Mater. Chem. A*, 2018, **6**, 15433.

92 W. Liu, X. Xu, J. Yuan, M. Leclerc, Y. Zou and Y. Li, *ACS Energy Lett.*, 2021, **6**, 598.

93 Y. Lin, F. Zhao, Q. He, L. Huo, Y. Wu, T. C. Parker, W. Ma, Y. Sun, C. Wang, D. Zhu, A. J. Heeger, S. R. Marder and X. Zhan, *J. Am. Chem. Soc.*, 2016, **138**, 4955.

94 W. Gao, Q. An, R. Ming, D. Xie, K. Wu, Z. Luo, Y. Zou, F. Zhang and C. Yang, *Adv. Funct. Mater.*, 2017, **27**, 1702194.

95 Y. Yang, Z. G. Zhang, H. Bin, S. Chen, L. Gao, L. Xue, C. Yang and Y. Li, *J. Am. Chem. Soc.*, 2016, **138**, 15011.

96 Z. Zhang, L. Feng, S. Xu, Y. Liu, H. Peng, Z. G. Zhang, Y. Li and Y. Zou, *Adv. Sci.*, 2017, **4**, 1700152.

97 M. Chang, Y. Wang, Y.-Q.-Q. Yi, X. Ke, X. Wan, C. Li and Y. Chen, *J. Mater. Chem. A*, 2018, **6**, 8586.

98 S. Lee, K. H. Park, J. H. Lee, H. Back, M. J. Sung, J. Lee, J. Kim, H. Kim, Y. H. Kim, S. K. Kwon and K. Lee, *Adv. Energy Mater.*, 2019, **9**, 1900044.

99 B. Zhao, W. Wang, J. Xin, H. Wu, H. Liu, Z. Guo, Z. Cong, W. Ma and C. Gao, *ACS Sustainable Chem. Eng.*, 2018, **6**, 2177.

100 C. Zhang, S. Feng, Y. Liu, R. Hou, Z. Zhang, X. Xu, Y. Wu and Z. Bo, *ACS Appl. Mater. Interfaces*, 2017, **9**, 33906.

101 J. Lee, E. M. Go, S. Dharmapurikar, J. Xu, S. M. Lee, M. Jeong, K. C. Lee, J. Oh, Y. Cho, C. Zhang, M. Xiao, S. K. Kwak and C. Yang, *J. Mater. Chem. A*, 2019, **7**, 18468.

102 Y. Xin, G. Zeng, J. OuYang, X. Zhao and X. Yang, *J. Mater. Chem. C*, 2019, **7**, 9513.

103 Z. Fei, F. D. Eisner, X. Jiao, M. Azzouzi, J. A. Rohr, Y. Han, M. Shahid, A. S. R. Chesman, C. D. Easton, C. R. McNeill, T. D. Anthopoulos, J. Nelson and M. Heeney, *Adv. Mater.*, 2018, **30**, 1705209.

104 L. Ye, K. Weng, J. Xu, X. Du, S. Chandrabose, K. Chen, J. Zhou, G. Han, S. Tan, Z. Xie, Y. Yi, N. Li, F. Liu, J. M. Hodgkiss, C. J. Brabec and Y. Sun, *Nat. Commun.*, 2020, **11**, 6005.

105 X. Liu, B. Xie, C. Duan, Z. Wang, B. Fan, K. Zhang, B. Lin, F. J. M. Colberts, W. Ma, R. A. J. Janssen, F. Huang and Y. Cao, *J. Mater. Chem. A*, 2018, **6**, 395.

106 B. Jang, C. Lee, Y. W. Lee, D. Kim, M. A. Uddin, F. S. Kim, B. J. Kim and H. Y. Woo, *Chin. J. Chem.*, 2018, **36**, 199.

107 Z. Zhang, J. Yu, X. Yin, Z. Hu, Y. Jiang, J. Sun, J. Zhou, F. Zhang, T. P. Russell, F. Liu and W. Tang, *Adv. Funct. Mater.*, 2018, **28**, 1705095.

108 Z. Zhang, H. Wang, J. Yu, R. Sun, J. Xu, L. Yang, R. Geng, J. Cao, F. Du, J. Min, F. Liu and W. Tang, *Chem. Mater.*, 2020, **32**, 1297.

109 Z. Zhang, S. Guang, J. Yu, H. Wang, J. Cao, F. Du, X. Wang and W. Tang, *Sci. Bull.*, 2020, **65**, 1533.

110 K. Feng, J. Huang, X. Zhang, Z. Wu, S. Shi, L. Thomsen, Y. Tian, H. Y. Woo, C. R. McNeill and X. Guo, *Adv. Mater.*, 2020, **32**, 2001476.

111 Y. Lin, Q. He, F. Zhao, L. Huo, J. Mai, X. Lu, C. J. Su, T. Li, J. Wang, J. Zhu, Y. Sun, C. Wang and X. Zhan, *J. Am. Chem. Soc.*, 2016, **138**, 2973.

112 X. Li, F. Pan, C. Sun, M. Zhang, Z. Wang, J. Du, J. Wang, M. Xiao, L. Xue, Z. G. Zhang, C. Zhang, F. Liu and Y. Li, *Nat. Commun.*, 2019, **10**, 519.

113 X. Li, H. Huang, I. Angunawela, J. Zhou, J. Du, A. Liebman-Pelaez, C. Zhu, Z. Zhang, L. Meng, Z. Xie, H. Ade and Y. Li, *Adv. Funct. Mater.*, 2019, **30**, 1906855.

114 Z. Luo, C. Sun, S. Chen, Z.-G. Zhang, K. Wu, B. Qiu, C. Yang, Y. Li and C. Yang, *Adv. Energy Mater.*, 2018, **8**, 1800856.

115 S. Feng, C. Zhang, Y. Liu, Z. Bi, Z. Zhang, X. Xu, W. Ma and Z. Bo, *Adv. Mater.*, 2017, **29**, 1703527.

116 Y. Li, N. Zheng, L. Yu, S. Wen, C. Gao, M. Sun and R. Yang, *Adv. Mater.*, 2019, **31**, 1807832.

117 Y. Li, L. Yu, L. Chen, C. Han, H. Jiang, Z. Liu, N. Zheng, J. Wang, M. Sun, R. Yang and X. Bao, *Innovation*, 2021, **2**, 100090.

118 C. Han, H. Jiang, P. Wang, L. Yu, J. Wang, J. Han, W. Shen, N. Zheng, S. Wen, Y. Li and X. Bao, *Mater. Chem. Front.*, 2021, **5**, 3050.

119 Y. Lin, Z.-G. Zhang, H. Bai, J. Wang, Y. Yao, Y. Li, D. Zhu and X. Zhan, *Energy Environ. Sci.*, 2015, **8**, 610.

120 H. Yao, Y. Chen, Y. Qin, R. Yu, Y. Cui, B. Yang, S. Li, K. Zhang and J. Hou, *Adv. Mater.*, 2016, **28**, 8283.

121 J. Lee, S. Song, J. Huang, Z. Du, H. Lee, Z. Zhu, S.-J. Ko, T.-Q. Nguyen, J. Y. Kim, K. Cho and G. C. Bazan, *ACS Mater. Lett.*, 2020, **2**, 395.

122 Y. Liu, M. Li, J. Yang, W. Xue, S. Feng, J. Song, Z. Tang, W. Ma and Z. Bo, *Adv. Energy Mater.*, 2019, **9**, 1901280.

123 Y. Liu, M. Li, X. Zhou, Q.-Q. Jia, S. Feng, P. Jiang, X. Xu, W. Ma, H.-B. Li and Z. Bo, *ACS Energy Lett.*, 2018, **3**, 1832.

124 S. Ming, C. Zhang, P. Jiang, Q. Jiang, Z. Ma, J. Song and Z. Bo, *ACS Appl. Mater. Interfaces*, 2019, **11**, 19444.

125 Z. Luo, Y. Zhao, Z. G. Zhang, G. Li, K. Wu, D. Xie, W. Gao, Y. Li and C. Yang, *ACS Appl. Mater. Interfaces*, 2017, **9**, 34146.

126 R. Qiu, Z. Wu, S. Li, H. Jiang, Q. Wang, Y. Chen, X. Liu, L. Zhang and J. Chen, *Sci. China Chem.*, 2021, **64**, 1208.

127 Y. Liu, Z. Zhang, S. Feng, M. Li, L. Wu, R. Hou, X. Xu, X. Chen and Z. Bo, *J. Am. Chem. Soc.*, 2017, **139**, 3356.

128 Z.-G. Zhang and Y. Li, *Sci. China Chem.*, 2014, **58**, 192.

129 Y. Li, H. Chen, H. Lai, X. lai, T. Rehman, Y. Zhu, Y. Wang, Q. Wu and F. He, *ACS Mater. Lett.*, 2022, **4**, 1322.

130 Y. Xu, H. Yao, L. Ma, J. Wang and J. Hou, *Rep. Prog. Phys.*, 2020, **83**, 082601.

131 J. Wang, W. Wang, X. Wang, Y. Wu, Q. Zhang, C. Yan, W. Ma, W. You and X. Zhan, *Adv. Mater.*, 2017, **29**, 1702125.

2756 | *Energy Environ. Sci.*, 2023, **16**, 2732–2758

This journal is © The Royal Society of Chemistry 2023

132 Y. Zhang, Y. Wang, T. Yang, T. Liu, Y. Xiao, X. Lu, H. Yan, Z. Yuan, Y. Chen and Y. Li, *ACS Appl. Mater. Interfaces*, 2019, **11**, 32218.

133 Y. Zhang, L. Shi, T. Yang, T. Liu, Y. Xiao, X. Lu, H. Yan, Z. Yuan, Y. Chen and Y. Li, *J. Mater. Chem. A*, 2019, **7**, 26351.

134 Y. Zhang, Y. Cho, L. Zhong, Y. Wang, B. Huang, Z. Yuan, C. Yang, Y. Chen and Y. Li, *Sol. RRL*, 2020, **4**, 2000071.

135 G.-Z. Yuan, H. Fan, S.-S. Wan, Z. Jiang, Y.-Q. Liu, K.-K. Liu, H.-R. Bai, X. Zhu and J.-L. Wang, *J. Mater. Chem. A*, 2019, **7**, 20274.

136 G. Li, J. Wu, J. Fang, X. Guo, L. Zhu, F. Liu, M. Zhang and Y. Li, *Chin. J. Chem.*, 2020, **38**, 697.

137 T. Liu, W. Gao, Y. Wang, T. Yang, R. Ma, G. Zhang, C. Zhong, W. Ma, H. Yan and C. Yang, *Adv. Funct. Mater.*, 2019, **29**, 1902155.

138 W. Gao, T. Liu, R. Ming, Z. Luo, K. Wu, L. Zhang, J. Xin, D. Xie, G. Zhang, W. Ma, H. Yan and C. Yang, *Adv. Funct. Mater.*, 2018, **28**, 1803128.

139 B. Kan, X. Chen, K. Gao, M. Zhang, F. Lin, X. Peng, F. Liu and A. K. Y. Jen, *Nano Energy*, 2020, **67**, 104209.

140 X. Chen, B. Kan, Y. Kan, M. Zhang, S. B. Jo, K. Gao, F. Lin, F. Liu, X. Peng, Y. Cao and A. K. Y. Jen, *Adv. Funct. Mater.*, 2020, **30**, 1909535.

141 D. Su, M.-A. Pan, Z. Liu, T.-K. Lau, X. Li, F. Shen, S. Huo, X. Lu, A. Xu, H. Yan and C. Zhan, *Chem. Mater.*, 2019, **31**, 8908.

142 D. Liu, L. Yang, Y. Wu, X. Wang, Y. Zeng, G. Han, H. Yao, S. Li, S. Zhang, Y. Zhang, Y. Yi, C. He, W. Ma and J. Hou, *Chem. Mater.*, 2018, **30**, 619.

143 D. Cai, J. Zhang, J.-Y. Wang, Y. Ma, S. Wan, P. Wang, Z. Wei and Q. Zheng, *J. Mater. Chem. A*, 2020, **8**, 24543.

144 Y. Ma, D. Cai, S. Wan, P. Yin, P. Wang, W. Lin and Q. Zheng, *Natl. Sci. Rev.*, 2020, **7**, 1886.

145 Y. Ma, M. Zhang, S. Wan, P. Yin, P. Wang, D. Cai, F. Liu and Q. Zheng, *Joule*, 2021, **5**, 197.

146 J. Sun, X. Ma, Z. Zhang, J. Yu, J. Zhou, X. Yin, L. Yang, R. Geng, R. Zhu, F. Zhang and W. Tang, *Adv. Mater.*, 2018, **30**, 1707150.

147 H. Feng, X. Song, M. Zhang, J. Yu, Z. Zhang, R. Geng, L. Yang, F. Liu, D. Baran and W. Tang, *Mater. Chem. Front.*, 2019, **3**, 702.

148 L. Yang, X. Song, J. Yu, H. Wang, Z. Zhang, R. Geng, J. Cao, D. Baran and W. Tang, *J. Mater. Chem. A*, 2019, **7**, 22279.

149 L. Yang, Z. Hu, Z. Zhang, J. Cao, H. Wang, J. Yu, F. Zhang and W. Tang, *J. Mater. Chem. A*, 2020, **8**, 5458.

150 J. Cao, S. Qu, L. Yang, H. Wang, J. Yu and W. Tang, *Sci. Bull.*, 2020, **65**, 1876.

151 J. Cao, H. Wang, S. Qu, J. Yu, L. Yang, Z. Zhang, F. Du and W. Tang, *Adv. Funct. Mater.*, 2020, **30**, 2006141.

152 H. Huang, Q. Guo, S. Feng, C. Zhang, Z. Bi, W. Xue, J. Yang, J. Song, C. Li, X. Xu, Z. Tang, W. Ma and Z. Bo, *Nat. Commun.*, 2019, **10**, 3038.

153 M. Chang, L. Meng, Y. Wang, X. Ke, Y.-Q.-Q. Yi, N. Zheng, W. Zheng, Z. Xie, M. Zhang, Y. Yi, H. Zhang, X. Wan, C. Li and Y. Chen, *Chem. Mater.*, 2020, **32**, 2593.

154 J. Huang, C.-Y. Gao, X.-H. Fan, X. Zhu and L.-M. Yang, *Energy Technol.*, 2021, **10**, 2100912.

155 S. Ye, S. Chen, S. Li, Y. Pan, X. Xia, W. Fu, L. Zuo, X. Lu, M. Shi and H. Chen, *ChemSusChem*, 2021, **14**, 3599.

156 J. Lee, S.-J. Ko, H. Lee, J. Huang, Z. Zhu, M. Seifrid, J. Vollbrecht, V. V. Brus, A. Karki, H. Wang, K. Cho, T.-Q. Nguyen and G. C. Bazan, *ACS Energy Lett.*, 2019, **4**, 1401.

157 X. Zhang, C. Li, L. Qin, H. Chen, J. Yu, Y. Wei, X. Liu, J. Zhang, Z. Wei, F. Gao, Q. Peng and H. Huang, *Angew. Chem., Int. Ed.*, 2021, **60**, 17720.

158 H. Huang, Q. Chen, Q. Guo, L. Wang, B. Wu, X. Xu, W. Ma, Z. Tang, C. Li and Z. Bo, *Dyes Pigm.*, 2023, **210**, 111033.

159 Y. Zhou, M. Li, S. Shen, J. Wang, R. Zheng, H. Lu, Y. Liu, Z. Ma, J. Song and Z. Bo, *ACS Appl. Mater. Interfaces*, 2021, **13**, 1603.

160 Y. Zhou, M. Li, H. Lu, H. Jin, X. Wang, Y. Zhang, S. Shen, Z. Ma, J. Song and Z. Bo, *Adv. Funct. Mater.*, 2021, **31**, 2101742.

161 Y. N. Chen, M. Li, Y. Wang, J. Wang, M. Zhang, Y. Zhou, J. Yang, Y. Liu, F. Liu, Z. Tang, Q. Bao and Z. Bo, *Angew. Chem., Int. Ed.*, 2020, **59**, 22714.

162 L. Ma, S. Zhang, J. Zhu, J. Wang, J. Ren, J. Zhang and J. Hou, *Nat. Commun.*, 2021, **12**, 5093.

163 X. Wang, H. Lu, J. Zhou, X. Xu, C. Zhang, H. Huang, J. Song, Y. Liu, X. Xu, Z. Xie, Z. Tang and Z. Bo, *ACS Appl. Mater. Interfaces*, 2021, **13**, 39652.

164 H. Lu, X. Wang, H. Wang, A. Zhang, X. Zheng, N. Yu, Z. Tang, X. Xu, Y. Liu, Y.-N. Chen and Z. Bo, *Sci. China Chem.*, 2022, **65**, 594.

165 K. Jiang, Q. Wei, J. Y. L. Lai, Z. Peng, H. K. Kim, J. Yuan, L. Ye, H. Ade, Y. Zou and H. Yan, *Joule*, 2019, **3**, 3020.

166 Z. Luo, R. Sun, C. Zhong, T. Liu, G. Zhang, Y. Zou, X. Jiao, J. Min and C. Yang, *Sci. China Chem.*, 2020, **63**, 361.

167 Y. Cui, H. Yao, L. Hong, T. Zhang, Y. Tang, B. Lin, K. Xian, B. Gao, C. An, P. Bi, W. Ma and J. Hou, *Natl. Sci. Rev.*, 2020, **7**, 1239.

168 D. Mo, H. Chen, J. Zhou, N. Tang, L. Han, Y. Zhu, P. Chao, H. Lai, Z. Xie and F. He, *J. Mater. Chem. A*, 2020, **8**, 8903.

169 J. Pan, Y. Shi, J. Yu, H. Zhang, Y. Liu, J. Zhang, F. Gao, X. Yu, K. Lu and Z. Wei, *ACS Appl. Mater. Interfaces*, 2021, **13**, 22531.

170 H. Chen, R. Zhang, X. Chen, G. Zeng, L. Kobera, S. Abbrent, B. Zhang, W. Chen, G. Xu, J. Oh, S.-H. Kang, S. Chen, C. Yang, J. Brus, J. Hou, F. Gao, Y. Li and Y. Li, *Nat. Energy*, 2021, **6**, 1045.

171 T. Li, K. Wang, G. Cai, Y. Li, H. Liu, Y. Jia, Z. Zhang, X. Lu, Y. Yang and Y. Lin, *JACS Au*, 2021, **1**, 1733.

172 S. Chen, L. Feng, T. Jia, J. Jing, Z. Hu, K. Zhang and F. Huang, *Sci. China Chem.*, 2021, **64**, 1192.

173 Y. J. Su, H. Nie, C. F. Chang, S. C. Huang, Y. H. Huang, T. W. Chen, K. K. Hsu, T. Y. Lee, H. M. Shih, C. W. Ko, J. T. Chen and C. S. Hsu, *ACS Appl. Mater. Interfaces*, 2021, **13**, 59043.

174 L. Wang, C. Guo, X. Zhang, S. Cheng, D. Li, J. Cai, C. Chen, Y. Fu, J. Zhou, H. Qin, D. Liu and T. Wang, *Chem. Mater.*, 2021, **33**, 8854.

This journal is © The Royal Society of Chemistry 2023

Energy Environ. Sci., 2023, **16**, 2732–2758 | 2757

175 J. Zhang, F. Bai, I. Angunawela, X. Xu, S. Luo, C. Li, G. Chai, H. Yu, Y. Chen, H. Hu, Z. Ma, H. Ade and H. Yan, *Adv. Energy Mater.*, 2021, **11**, 2102596.

176 Y. Chang, J. Zhang, Y. Chen, G. Chai, X. Xu, L. Yu, R. Ma, H. Yu, T. Liu, P. Liu, Q. Peng and H. Yan, *Adv. Energy Mater.*, 2021, **11**, 2100079.

177 X. Kong, C. Zhu, J. Zhang, L. Meng, S. Qin, J. Zhang, J. Li, Z. Wei and Y. Li, *Energy Environ. Sci.*, 2022, **15**, 2011.

178 P. Tan, L. Liu, Z. Y. Chen, H. Lai, Y. Zhu, H. Chen, N. Zheng, Y. Zhang and F. He, *Adv. Funct. Mater.*, 2021, **31**, 2106524.

179 B. Fan, W. Gao, R. Zhang, W. Kaminsky, F. R. Lin, X. Xia, Q. Fan, Y. Li, Y. An, Y. Wu, M. Liu, X. Lu, W. J. Li, H.-L. Yip, F. Gao and A. K.-Y. Jen, *J. Am. Chem. Soc.*, 2023, **145**, 5909.

180 Y. Chen, F. Bai, Z. Peng, L. Zhu, J. Zhang, X. Zou, Y. Qin, H. K. Kim, J. Yuan, L. K. Ma, J. Zhang, H. Yu, P. C. Y. Chow, F. Huang, Y. Zou, H. Ade, F. Liu and H. Yan, *Adv. Energy Mater.*, 2020, **11**, 2003141.

181 Y. Chen, R. Ma, T. Liu, Y. Xiao, H. K. Kim, J. Zhang, C. Ma, H. Sun, F. Bai, X. Guo, K. S. Wong, X. Lu and H. Yan, *Adv. Energy Mater.*, 2021, **11**, 2003777.

182 A. M. H. Cheung, H. Yu, S. Luo, Z. Wang, Z. Qi, W. Zhou, L. Arunagiri, Y. Chang, H. Yao, H. Ade and H. Yan, *J. Mater. Chem. A*, 2020, **8**, 23239.

183 C. Xiao, X. Wang, T. Zhong, R. Zhou, X. Zheng, Y. Liu, T. Hu, Y. Luo, F. Sun, B. Xiao, Z. Liu, C. Yang and R. Yang, *Adv. Sci.*, 2023, **10**, 2206580.

184 Z. Li, C. Zhu, J. Yuan, L. Zhou, W. Liu, X. Xia, J. Hong, H. Chen, Q. Wei, X. Lu, Y. Li and Y. Zou, *J. Energy Chem.*, 2022, **65**, 173.

185 H. Chen, X. Xia, J. Yuan, Q. Wei, W. Liu, Z. Li, C. Zhu, X. Wang, H. Guan, X. Lu, Y. Li and Y. Zou, *ACS Appl. Mater. Interfaces*, 2021, **13**, 36053.

186 F. Qi, K. Jiang, F. Lin, Z. Wu, H. Zhang, W. Gao, Y. Li, Z. Cai, H. Y. Woo, Z. Zhu and A. K. Y. Jen, *ACS Energy Lett.*, 2020, **6**, 9.

187 F. Qi, L. O. Jones, K. Jiang, S. H. Jang, W. Kaminsky, J. Oh, H. Zhang, Z. Cai, C. Yang, K. L. Kohlstedt, G. C. Schatz, F. R. Lin, T. J. Marks and A. K. Jen, *Mater. Horiz.*, 2022, **9**, 403.

188 Y. Li, H. Chen, H. Lai, X. lai, T. Rehman, Y. Zhu, Y. Wang, Q. Wu and F. He, *ACS Mater. Lett.*, 2022, **4**, 1322.

189 J. Wang, X. Jiang, H. Wu, G. Feng, H. Wu, J. Li, Y. Yi, X. Feng, Z. Ma, W. Li, K. Vandewal and Z. Tang, *Nat. Commun.*, 2021, **12**, 6679.